Università degli Studi di Napoli

Federico II

Dipartimento di Medicina Clinica e Chirurgia

Dottorato in Terapie Avanzate

Biomediche e Chirurgiche

(ciclo XXXII)

Thyroid hormone metabolism plays stage-specific roles in Squamous Cell Carcinoma (SCC) tumor progression

Caterina Miro

Tutor:

Prof. Domenico Salvatore

INDEX

1. Summary

1.1 The modulation of intracellular action of thyroid hormone in Squamous Cell Carcinomas (SCCs)

Squamous cell carcinoma (SCC) is the second most frequent cancer worldwide and entails a substantial risk of metastasis. Thyroid hormone (TH) signalling regulates the metabolism, growth and differentiation of all cell types and tissues, and thus strongly impacts on cancer. However, our understanding of the effects exerted by TH on tumor formation and progression remains limited.

Intracellular TH concentration is not simply the mirror of circulating TH levels but is regulated in the target tissues by a balance between the activating and inactivating deiodinases enzymes, D2 and D3 which provide the ability to fine-tune TH action at cell level. TH deregulation is frequent in human tumors, in particular type 3 iodothyronine deiodinase (D3), the thyroid hormone (TH)-inactivating enzyme, is overexpressed in hyper-proliferating contexts and in cancer. Studies from our group demonstrated that, by terminating TH action within the tumor microenvironment, D3 enhances cancer cell proliferation.

The aim of my PhD thesis has been to understand how the TH regulation by the cell-specific action of its inactivating enzyme, D3, regulates multiple aspects of tumorigenesis, ranging from cancer formation to progression. Epithelial tumors arise through a multistep process in which invasion and metastasis often depend on the cancer cell epithelial-mesenchymal transition (EMT). We observed that the D3-mediated activation of the intracellular thyroid hormone (TH) signal promotes the EMT and malignant evolution of squamous cell carcinoma (SCC) cells. TH induces the EMT by transcriptionally up-regulating ZEB-1, mesenchymal genes and metalloproteases and suppresses E-cadherin expression. Our study establishes a new role for TH in the tumorigenic process and describes a novel connection between a metabolic hormone and the invasive proclivity of SCC. Moreover, our data indicate that tumor progression depends on precise T3 availability and provide the rationale for the concept that pharmacological inactivation of TH signal reduces the progression and invasiveness of SCC, and probably of other hormone-sensitive carcinomas.

2. Introduction

2.1 Squamous Cell Carcinoma (SCCs)

Nonmelanoma skin cancer (NMSC), comprising squamous cell carcinomas (SCCs) and basal cell carcinoma (BCCs), is by far the most common cancer among Caucasian people, with a recorded incidence in 2006 of more than 3 million in the U.S. alone [1] .

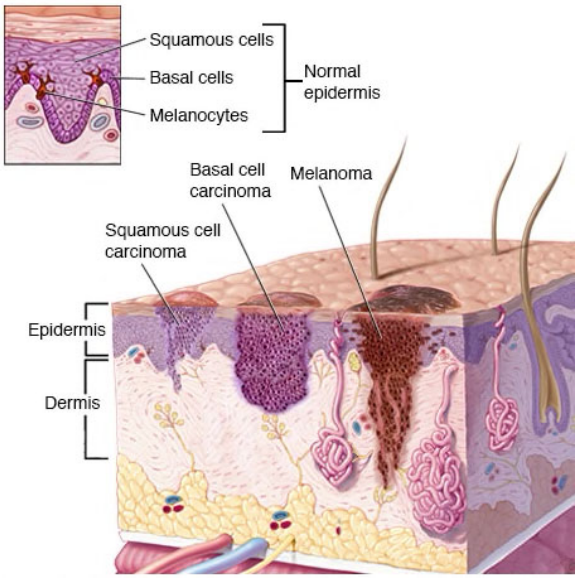

Figure 1

Types of skin cancer

The difference between BCC, SCC, and melanoma is the type of cell from which each arises and how far they penetrate the skin. BCC is thought to derive from skin stem cells within the hair follicle. SCC is a cancer of the keratinocyte (the most common cell in the epidermis, the outermost layer of the skin), and melanoma forms from melanocytes (skin cells in the bottom layer of the epidermis).

Basal cell carcinoma (BCC) accounts for 75% of cases and is a slow-growing, locally invasive epidermal tumour with a metastatic rate of <0.1% [2]. Squamous cell carcinoma (SCC) accounts for the majority of the remainder of cases of NMSC and arises from dysplastic epidermal keratinocytes [3]. In contrast to BCC, SCC has a significant recognised rate of metastasis (0.3–3.7%), the majority of which occurs within a subgroup of high-risk SCC.

The incidence of SCCs is sharply rising owing to increased exposure to carcinogens, such as ultraviolet radiation related to sun exposure, smoking, alcohol consumption or human papilloma virus (HPV) infection. SCCs are classified according to the location where they

appear, being frequently found in skin, head and neck, oesophagus, lung and cervix and more rarely in pancreas, thyroid, bladder and prostate.

Cutaneous squamous cell carcinoma (cSCC) is the second most common malignancy in fair-skinned individuals behind BCC [4]. cSCC rarely metastasize (5%), but metastasis is associated with a poor prognosis, with only a 10–20% survival rate over 10 years [5]. Although most nonmelanoma skin cancer can be successfully treated with surgery and/or chemotherapy, metastatic SCC is correlated with an extremely poor long-term prognosis [6]. To develop better clinical treatments and chemoprevention strategies for SCC, there is a need to achieve a better understanding of the biology of the disease through the development of animal models that recapitulate human cSCC, crucial for understanding the molecular pathogenesis of these tumors.

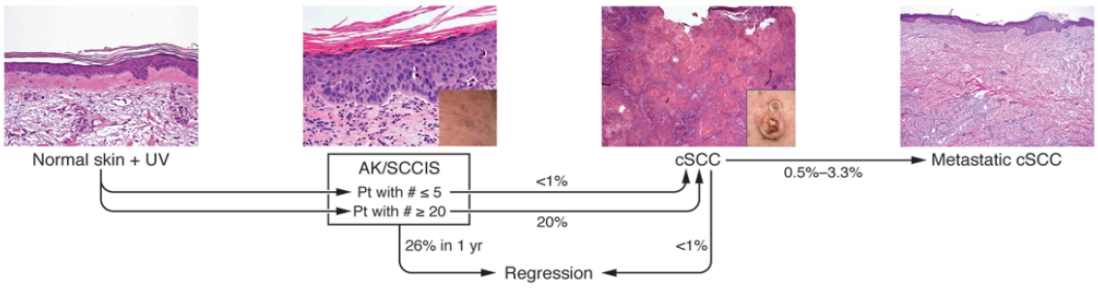

Figure 2
Sequence of Events Thought to Occur after Ultraviolet (UV) Irradiation of the Skin.
Probability that human cutaneous neoplastic lesions will progress to invasive carcinoma**.**

SCC development through the canonical carcinogenesis model in mice comprises a multistep progression process starting from the precancerous actinic keratosis (AK) in which keratinocyte atypia is confined to only a portion of the epidermis leading to abnormal differentiation and stratum corneum thickening with retained nuclei. When keratinocyte atypia progresses to include the entire epidermis, the lesion is defined as SCC in situ (SCCis) [7].

Approximately 26% of AK/SCCis spontaneously regress in 1 year however in patients with greater than 20 lesions, approximately 20% develop invasive histologic features and become SCC (Figure 2) [8, 9]. Mutations in p53, an important tumor suppressor whose inactivation has been implicated in a variety of tumors, have been identified in UV exposed skin as well as the majority of AK/SCCis [10-12]. Inactivating mutations in this

tumor suppressor can lead to genomic instability and loss of cell cycle regulation resulting in a greater propensity for development of additional mutations in oncogenes that drive carcinogenesis [13, 14]. Characterization of p53 null mice (p53–/–) demonstrated an increased propensity for lymphoma and sarcoma but not primary cutaneous tumors [15, 16]. However, in the presence of chronic UV exposure, p53–/– mice form AK and SCC-like tumors supporting the role of UV in the pathogenesis of cSCC (Figure 3) [16].

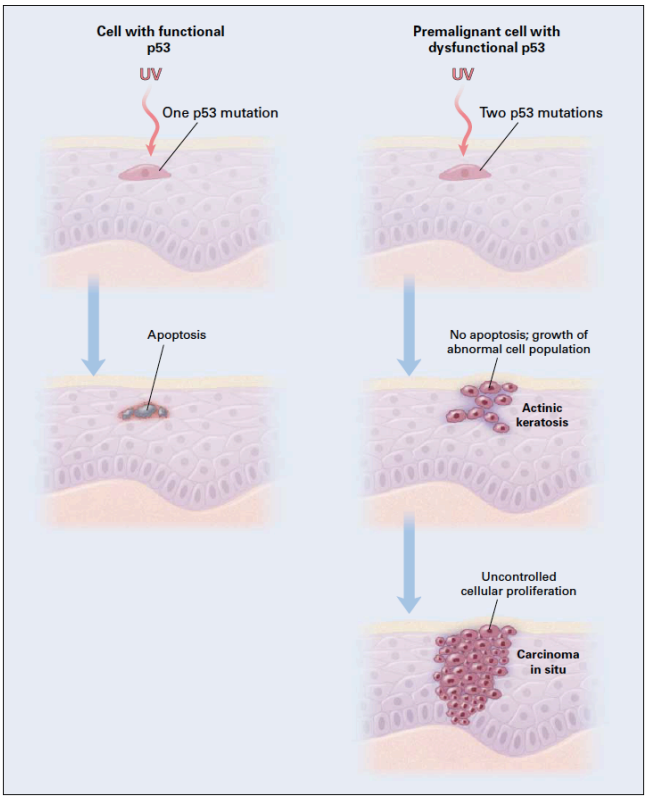

Figure 3

Sequence of Events Thought to Occur after Ultraviolet (UV) Irradiation of the Skin.

Ultraviolet radiation generates specific mutations (the formation of thymidine dimers) in the p53 tumor-suppressor gene. C-to-T transitional changes at pyrimidine sites, including CC-to-TT double-base changes, are the most frequent form of nucleotide-base substitution in ultraviolet-B–damaged DNA sequences. Keratinocytes with one mutation in p53 after ultraviolet irradiation undergo apoptosis. In contrast, keratinocytes with dysfunctional p53 and an additional p53 mutation as a result of irradiation cannot undergo apoptosis and instead undergo clonal expansion, which is manifested clinically as the development of an actinic keratosis. Uncontrolled proliferation of abnormal cells leads to squamous-cell carcinoma in situ and invasive squamous cell carcinoma.

Mouse models of SCC tumor formation through chemical carcinogenesis resemble human skin cancers and offer an ideal model to study cancer initiation and growth [17]. The most extensively used mouse cancer model is the multi-stage chemically induced skin tumours [18], which represents one of the best-established in vivo models for the study of the sequential and stepwise development of tumors (Figure 4). In addition, this model can be used to evaluate both novel skin cancer prevention strategies, and the impact of genetic background and genetic manipulation on tumor initiation, promotion and progression.

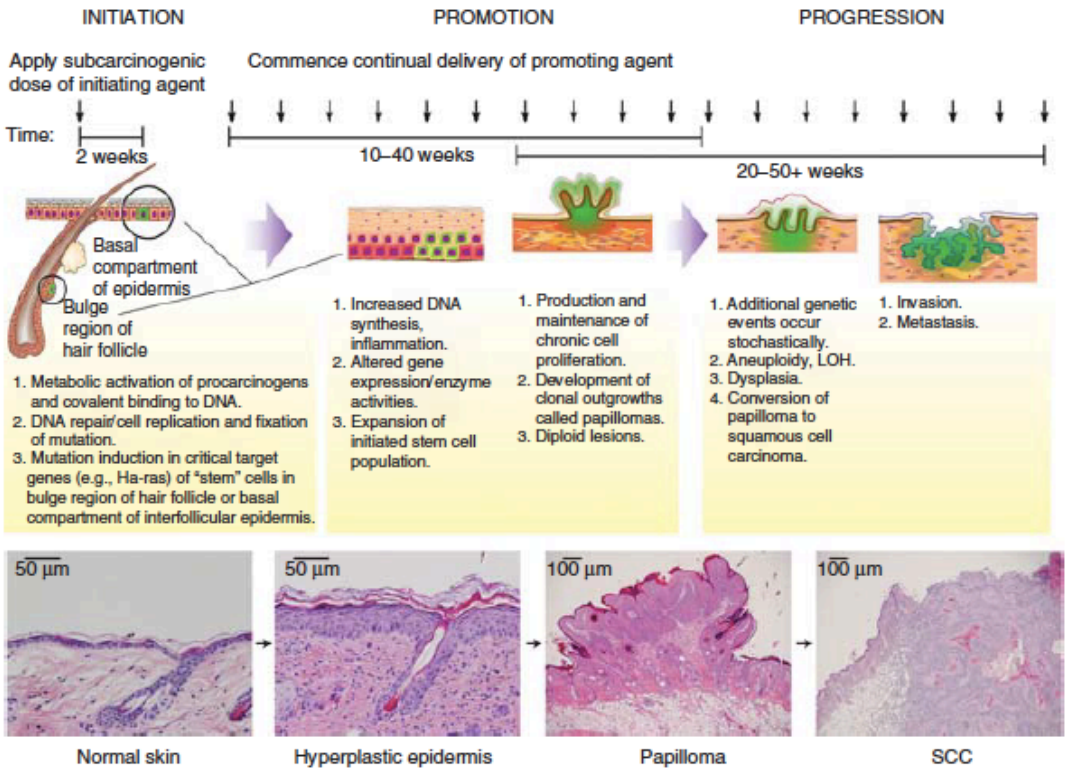

Figure 4

Two-stage model of skin carcinogenesis in mice.

During initiation, topical application of a sub-carcinogenic dose of a mutagenic agent induces mutations in target genes in keratinocyte stem cells. Repeated topical application of a promoting agent begins 2 weeks after initiation and continues for the duration of the study. Papillomas begin to arise after 6–12 weeks of promotion and a fraction begin to convert to squamous cell carcinoma (SCC) after 20 weeks. Representative H&E stained sections of normal skin, hyperplastic skin, a papilloma and a SCC are presented. All mice were handled in accordance with institutional and national regulations.

In the first step of multi-stage chemical carcinogenesis (called 'initiation'), mice are treated with a low dose of the mutagen 9,10-dimethyl-1,2-benzanthracene (DMBA). In

the second step (called 'promotion'), mice are treated with 12-O-tetradecanoyl phorbol-13-acetate (TPA), a drug that stimulates epidermal proliferation. During promotion, benign tumors (papillomas) arise, probably as a consequence of additional mutations, some of which will progress into invasive SCC. Interestingly, papillomas often contain activating mutations in *HRas* gene, suggesting that this mutation confers a selective advantage to epithelial cells [19]. However, not all papillomas contain mutations in the *HRas* gene, and some papillomas and SCC in both mouse and human present mutations in the *KRas* gene instead [20, 21]. Whereas Ras mutations seem to be an early step in skin cancer initiation, p53 mutations are associated with malignant progression [17, 22].

The first links between chemical exposure and the development of skin cancers prompted early attempts to develop tractable models for the study of chemically induced skin cancers. Chemical carcinogenesis of the skin has since emerged as the workhorse model of SCC, having been used to test hundreds of individual hypotheses across a wide range of topics in cancer biology. It played a pivotal role in the evolution of the concept of multi-stage carcinogenesis, as commonly applied to both human and mouse cancers, and has given rise to the operational definitions of the key tumor processes of initiation, promotion and malignant progression [23].

2.2 Molecular mechanisms of Epithelial–Mesenchymal Transition (EMT).

The idea that epithelial cells can downregulate epithelial characteristics and acquire mesenchymal characteristics arose in the early 1980s from observations made by Elizabeth Hay [24], who described epithelial to mesenchymal phenotype changes in the primitive streak of chick embryos. Initially described as 'epithelial to mesenchymal transformation', this differentiation process is now commonly known as epithelial–mesenchymal transition (EMT) to emphasize its transient nature; mesenchymal–epithelial transition (MET) describes the reverse process. The ability of epithelial cells to transition into mesenchymal cells and back, either partially or fully, illustrates an inherent plasticity of the epithelial phenotype. During EMT, epithelial cells lose their junctions and apical–basal polarity, reorganize their cytoskeleton, undergo a change in the signalling programmes that define cell shape and they reprogramme gene expression; this increases the motility of individual cells and enables the development of an invasive phenotype [25, 26].

A hallmark of EMT is the downregulation of E-cadherin to reinforce the destabilization of adherens junctions. Additionally, the repression of genes encoding claudins and occludin, and desmoplakin and plakophilin, stabilizes the dissolution of apical tight junctions and desmosomes, respectively [27]. These changes in gene expression prevent the de novo formation of epithelial cell–cell junctions and result in the loss of the epithelial barrier function [28]. The repression of genes encoding epithelial junction proteins is accompanied by the activation of genes, which promote mesenchymal adhesion. Specifically, the downregulation of E-cadherin is balanced by the increased expression of mesenchymal neural cadherin (N-cadherin), which results in a 'cadherin switch' that alters cell adhesion [25, 29].

Remodelling of the ECM and changes to cell interactions with the ECM are essential in the initiation and progression of EMT. Integrin complexes enable cells to receive signals from ECM proteins through interactions with signalling mediators, such as integrin-linked kinase (ILK), particularly interesting new Cys–His protein 1 (PINCH; also known as LIMS1) and parvin [29, 30]. As epithelial cells differentiate into mesenchymal cells, they do not interact with a basement membrane and communicate with a different ECM. Therefore, the cells downregulate some epithelial integrins, but activate the expression of

others; some of these newly expressed integrins have key roles in EMT progression. Changes to the integrin repertoire during EMT correlate with the increased expression of proteases, such as the matrix metalloproteinases MMP2 and MMP9, thus enhancing ECM protein degradation and enabling invasion [31]. MMPs additionally target some transmembrane proteins, which results in, for example, the release of the extracellular domain of E-cadherin, hence contributing to the loss of adherens junctions [31]. Some proteases that mediate invasion and some integrins, such as αvβ6, activate the differentiation factor TGFβ that is stored in a latent form in the ECM [32]. This exposes the cells to increased TGFβ signalling, which promotes EMT and stimulates the expression of some ECM proteins, such as collagens and fibronectin, enhancing the remodelling of the ECM into a matrix with a different composition and properties [25, 26].

The changes in gene expression that contribute to the repression of the epithelial phenotype and activation of the mesenchymal phenotype involve master regulators, including SNAIL, TWIST and zinc-finger E-box binding (ZEB) transcription factors. Their expression is activated early in EMT, and they thus have central roles in development, fibrosis and cancer. As these transcription factors have distinct expression profiles, their contributions to EMT depend on the cell or tissue type involved and the signalling pathways that initiate EMT. They often control the expression of each other and functionally cooperate at target genes [28], and additional transcription factors further define the EMT transcription programme and drive EMT progression.

Together, the EMT transcription factors coordinate the repression of epithelial genes and the induction of mesenchymal genes, and often the same transcription factors direct both repression and activation [33].

2.3 ZEB transcription factors.

Zinc finger E-box binding homeobox 1 (ZEB1) is a transcription factor that promotes tumor invasion and metastasis by inducing epithelial-mesenchymal transition (EMT) in carcinoma cells [34].

The mechanism of ZEB1-induced EMT mediation is that it is linked to the promoter region of the epithelial cell marker protein E-cadherin, inhibiting its transcriptional expression, causing the cells to lose epithelial properties.

ZEB1-induced EMT enhanced the loss of epithelial cell adhesion and polarity, induces drives growth and cytoskeleton remodeling, migration, metastasis and invasion [34]. ZEB1 is expressed at a strong intensity in the malignant cells at the edge of the tumor in most of invasive area and this expression is accompanied by a decreased membranous expression of E-cadherin.

Expression of ZEB1 (also named TCF8 or DeltaEF1) is regulated by multiple signaling pathways, such as WNT [35], NF-KB [36], TGF-β [37], COX2 [38], HIF signaling [39] and microRNAs [40, 41]. ZEB1 belongs to the ZEB family of transcription factors characterized by the presence of 2 zinc finger clusters, which are responsible for DNA binding, and a centrally located homeodomain. In addition, ZEB1 contains other protein-binding domains including the Smad interaction domain (SID), CtBP interaction domain (CID) and p300-P/CAF binding domain (CBD) [28, 42]. Through zinc finger clusters, ZEB1 can bind to specific DNA sequences named E-boxes [28]. By recruiting co-suppressors or co-activators through CID, SID or CBD, ZEB1 can either downregulate or upregulate the expression of its target genes [42]. For instance, ZEB1 directly binds to the E-box located in the promoter of CDH1, the gene encoding E-cadherin [43] and recruits the CtBP transcriptional co-repressors [44] and/or the SWI/SNF chromatin-remodeling protein BRG1 [45], leading to repression of CDH1 transcription and induction of EMT. On the other hand, by recruiting p300-P/CAF and Smad proteins, ZEB1 can activate the transcription of TGF-β-responsive genes and promote osteoblastic differentiation [42, 46].

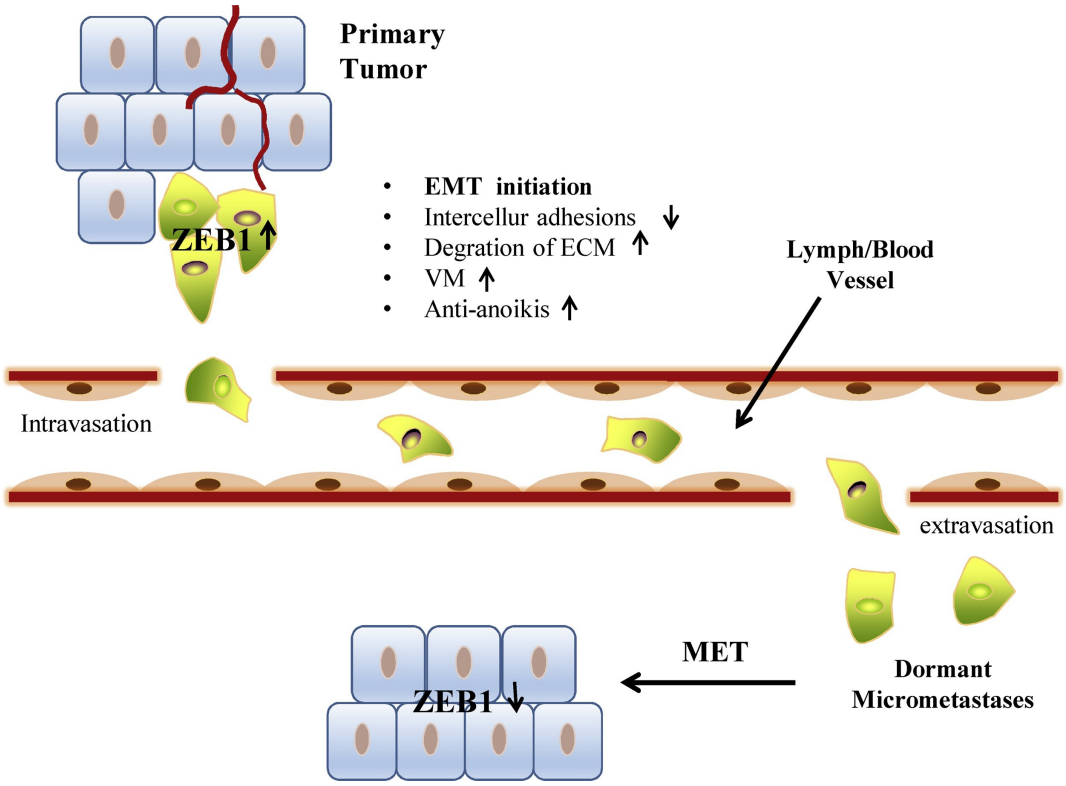

Figure 5.

The process of ZEB1 in tumor invasion and metastasis.

In response to EMT stimulating signal, ZEB1 level rises briefly to initiate EMT in cancer cells near or at the invasive, leading to edge of a primary tumor, loss of cell adhesion, degradation of ECM and formation of VM. As metastatic cells migrate away from the primary tumor, they lose ZEB1 expression.

2.4 Thyroid hormone action and deiodinases

Thyroid hormones (THs), triiodothyronine (T3), and thyroxine (T4), are involved in different biological processes as cell growth, development, differentiation, and the regulation of metabolism and homeostasis [47].

In the bloodstream, the steady-state level of TH concentration is regulated by the hypothalamic-pituitary-thyroid (HPT) axis. Hypothalamic thyroid releasing-hormone (TRH) stimulates thyrotrophic cells in the anterior pituitary to produce thyroid stimulating-hormone (TSH). In turn, TSH induces the production of pro-hormone thyroxine (T4) and-to a lesser extent-the active form triiodothyronine (T3) by the thyroid gland [48]. Secreted THs are released into the circulation and carried bound to proteins such as thyroxin binding globulin, transthyretin or serum albumin [49].

Besides systemic regulation, the TH concentration in target tissues can differ remarkably depending on local TH metabolism, which ultimately regulates target gene expression.

To exert its functions, TH must overcome several check-points, namely TH transporters, TH-metabolizing enzymes (deiodinases), TH receptors (TRs), and their interactions with co-repressors and co-activators [50]. Once TH enters the bloodstream, a low amount of TH, not bound to circulating transport proteins, is free to act on target cells.

The access of TH to the intracellular compartment is mediated by four different families of TH-transporting proteins that have been shown to be involved in the traffic of iodothyronines across the cell membrane [51-53]. These transporters are differentially expressed in tissues in a developmental and cell-type-specific fashion and, while most of them accept a variety of ligands, others have elevated substrate specificity [51, 54].

Among the most important thyroid hormone transporters are MCT8 and MCT10. The monocarboxylate 8 (MCT8) is probably the most relevant transporter as mutations in the MCT8 protein have been associated with variable levels of mental retardation in humans combined with lack of speech development, muscle hypotonia and endocrine dysfunctions [51, 55].

MCT8 transports both T4 and T3 and is expressed in liver, muscle, kidney and in many brain areas [56, 57], whereas the monocarboxylate 10 (MCT10) preferentially transports T3 instead of T4 and is expressed in kidney, liver and muscle [51]. Once transported into the cell, thyroid hormones can be metabolised by outer or inner ring deiodination through

the iodothyronine deiodinases, a selenocysteine-containing enzyme family consisting of three types: type 1 (DIO1), type 2 (DIO2) and type 3 (DIO3) (Figure 6) [58].

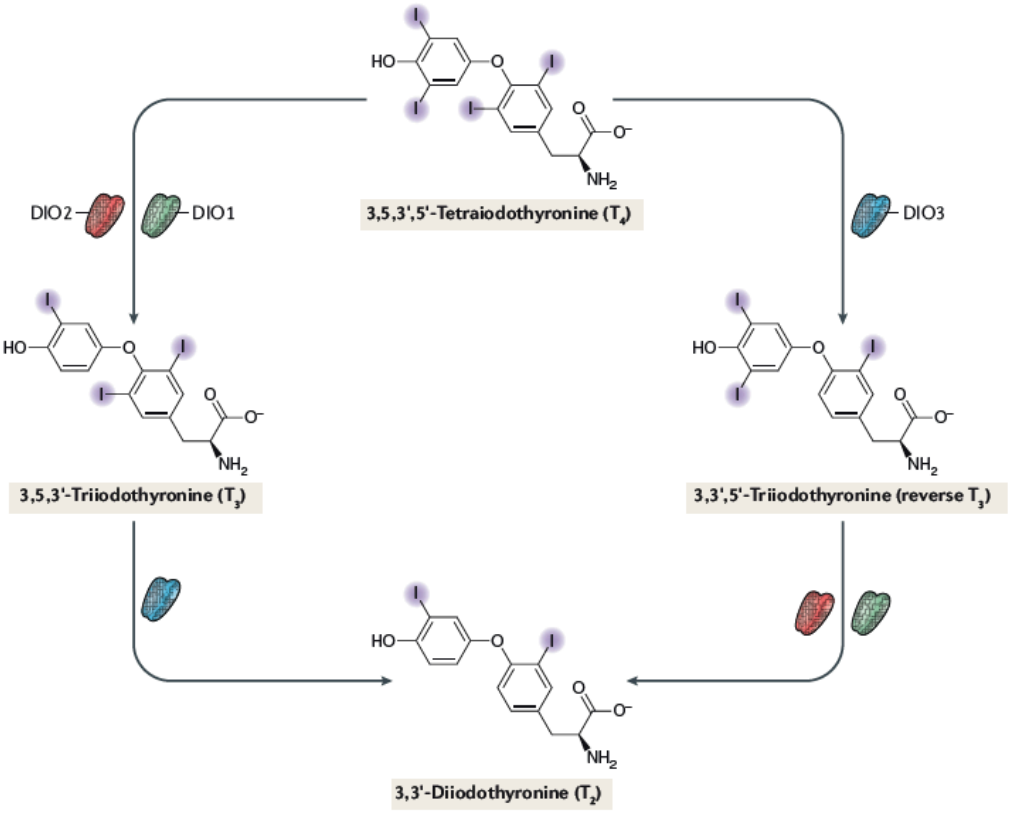

Figure 6

Deiodinase thyroid hormone action.

The pro-hormone T4 is activated by monodeiodination of the phenolic thyronine ring consequent to the action of DIO1 or DIO2 to form T3. Deiodination of the tyrosyl ring by DIO1 or DIO3 inactivates T4 and T3. Additional monodeiodination reactions generate reverse T3 (through DIO3-mediated T4 deiodination) and T2 (through DIO1-mediated and DIO2-mediated T3 deiodination). Reverse T3 cannot bind to the receptor and is thus considered an inactive metabolite. T2 is not involved in the genomic action of T3, but it might exert various metabolic effects.

All deiodinases are membrane-anchored proteins of 29–33 kDa that share substantial sequence homology, catalytic properties and contain the selenocysteine (Sec) aminoacid as the key residue within their catalytic center [59]. All the three deiodinases are homodimers whose dimerization is required for full catalytic activity [60, 61]. The unique feature of selenoproteins in general, and deiodinases in particular, lies in the recoding of the UGA codon from a stop codon to Sec-insertion codon by the presence of the SECIS element in the 3′ UTR of the respective mRNAs. Iodinated contrast agents such as iopanoic acid inhibit all three deiodinases, while propylthiouracil is a relatively specific inhibitor for DIO1 [59].

DIO1 is localized in the plasma membrane and is able to exert both activating and inactivating functions. DIO2 is localized in the endoplasmic reticulum and the DIO2 enzyme is considerably more efficient than DIO1: it catalyses the removal of an outer ring iodine atom from the pro-hormone T4 to generate the physiologically active product T3 [62, 63]. DIO1 is expressed in the thyroid, liver and kidneys, whereas DIO2 contributes to T3 production in the central nervous system, thyroid, skeletal muscle and brown adipose tissue [64].

DIO3 is localized in the plasma membrane and is the terminating enzyme, which irreversibly inactivates T3 and prevents T4 activation by catalysing the removal of an inner ring iodine atom, generating inactive metabolites that do not interact with T3 receptors, reverse triiodothyronine (rT3) and 3,3'-diiodothyronine (T2), respectively [65, 66] (Figure 7).

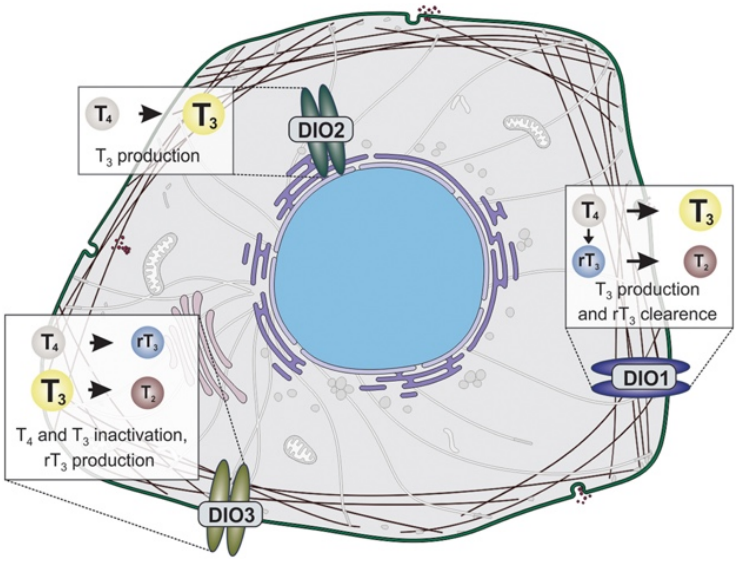

Figure 7

Types 1, 2, and 3 iodothyronine selenodeiodinases.

DIO1 is localized in the plasma membrane and is able to exert both activating and inactivating functions of TH. DIO2 is localized is localized in the endoplasmic reticulum and contributes to T3 production from the pro-hormone T4. DIO3, the TH-inactivating enzyme, is localized in the plasma membrane.

DIO3 is highly expressed in placenta and plays an important role during embryonic development protecting the fetus from excessive exposure to active thyroid hormone. DIO3 is also expressed in the brain and skin, but in adult healthy tissues expression levels are very low.

However, under specific pathophysiological conditions, its expression can be induced in other tissues [67] and is correlated with hyperproliferation conditions as cancer.

Therefore, depending on whether the deiodination occurs on the inner (IDR) or outer ring (ODR) of the iodothyronine substrate, the deiodination results in activating pathway or inactivating pathway.

Currently, tissue thyroid hormone concentrations are thought to be determined by the balance between deiodinases present in the tissue rather than by serum TH concentrations alone. Thus, the TH-inactivating enzyme impedes thyroid hormone access to specific tissues at critical times and prevents TH receptor saturation [68].

Once the active hormone T3 is present inside the cells, the classical mechanism of action of THs is mediated by the binding of T3 to nuclear receptors (TRs), a family of ligand-dependent transcription factors that enhance or inhibit the expression of target genes by binding to specific DNA sequences, known as TH response elements (TREs).

Thyroid hormone receptors exist in two isoforms, TRα and TRβ, which are encoded by the THRA and THRB genes, respectively [50].

The binding of T3 to TRs promotes a conformational change that induces the exchange of corepressors for coactivators, thus leading to gene transcription on responsive genes, a process known as the genomic effect of thyroid hormones [69, 70].

Besides the genomic action of THs, a second mechanism of TH actions is constituted by the non-genomic effects of thyroid hormones, which involves the binding of T3 or T4 to cellular proteins and interactions of thyroid hormone receptor with cellular partners [50]. Importantly, although these cytosolic interactions of thyroid hormone or thyroid hormone receptor are collectively called non-genomic actions, they might culminate in transcriptional activation of target genes [71].

2.5 The relationship between thyroid hormone and skin

The skin, as the primary interface between the body and the environment, provides a first line of defence against microbial pathogens and physical and chemical insults.

In mammals, epidermal development is a multistage process consisting of epidermal specification, commitment, stratification and terminal differentiation, as well as morphogenesis of its derivatives. To accomplish these feats, the epidermis constantly replenishes itself, thanks to the presence of stem cells that are capable of self-renewal and of producing transiently amplifying progenitor cells [72].

Human skin has two main compartments: the epidermis and the dermis (Figure 8).

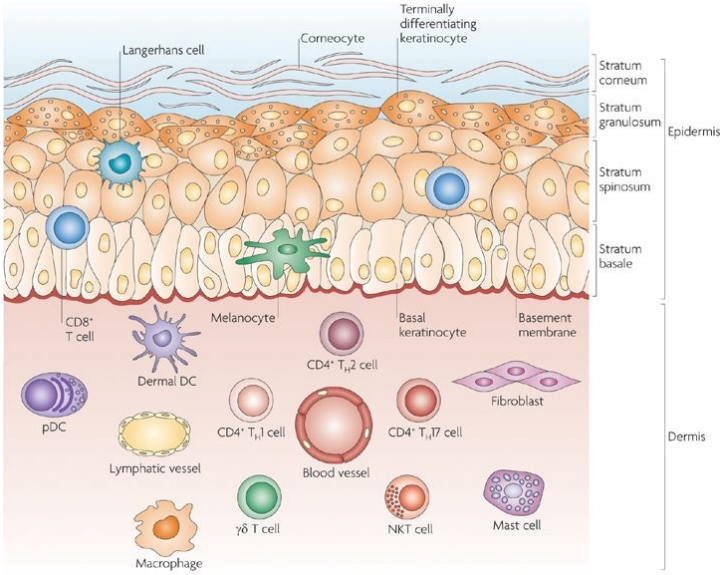

Figure 8

Skin anatomy and cellular effectors.

The structure of the skin reflects the complexity of its functions as a protective barrier: the epidermis contains the stratum basale, the stratum spinosum, the stratum granulosum and the outermost layer, the stratum corneum, which is responsible for the vital barrier function of the skin. Specialized cells in the epidermis include melanocytes, which produce pigment (melanin), and Langerhans cells. Rare T cells, mainly CD8+ cytotoxic T cells, can be found in the stratum basale and stratum spinosum. The dermis is composed of collagen, elastic tissue and reticular fibers. It contains many specialized cells, such as dendritic cell (DC) subsets, including dermal DCs and plasmacytoid DCs (pDCs), and T cell subsets, including CD4+ T helper 1 (TH1), TH2 and TH17 cells, γδ T cells and natural killer T (NKT) cells. In addition, macrophages, mast cells and fibroblasts are present. Blood and lymphatic vessels and nerves (not shown) are also present throughout the dermis.

The epidermis is the outer compartment and contains four strata. The stratum basale is the bottom layer of the epidermis and is responsible for the constantly renewing of the epidermal cells. This layer contains just one row of undifferentiated epidermal cells,

known as basal keratinocytes, that divide frequently. Basal keratinocytes differentiate and move to the next layer (the stratum spinosum; also known as the prickle cell layer) to begin a maturation process, but also divide to replenish the basal layer. Cells that move into the stratum spinosum change from being columnar to being polygonal in shape and start to synthesize keratins that are distinct from the basal-layer keratins. Keratinocytes in the stratum granulosum are characterized by dark clumps of cytoplasmic material and these cells actively produce keratin proteins and lipids. The stratum corneum, as the ultimate product of maturing keratinocytes, is the outermost of the four strata of the epidermis and is largely responsible for the barrier function of the skin. Cells in this layer, known as corneocytes, are dead keratinocyte-derived cells that are devoid of organelles. Keratinocytes of the basal layers express basal keratins K5 and K14; as cells exit from the basal layer and begin their journey towards the skin surface, they switch from the expression of keratins K14 and K5 to K1 and K10 [73]. The first suprabasal cells are known as spinous cells, reflecting their cytoskeleton of K1/K10 filament bundles connected to robust cell–cell junctions known as desmosomes. K6, K16 and K17 are also expressed suprabasally, but only in hyperproliferative situations such as wound healing (Figure 9) [73].

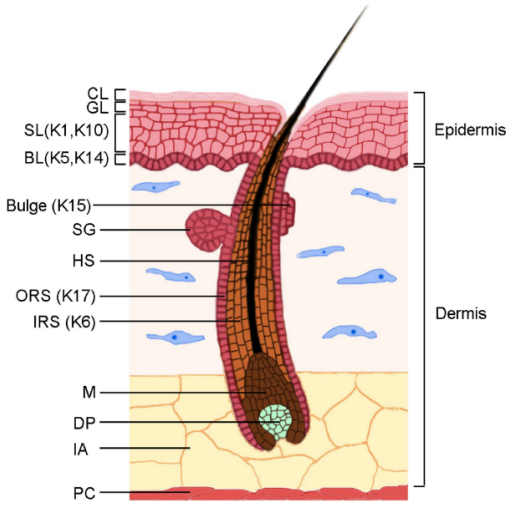

Figure 9

Skin structure

The epidermis is constituted by an undifferentiated basal layer (BL) of cells that progressively differentiate in the spinous layer (SL), granular layer (GL), and the cornified layer (CL). The HF consists of an outer root sheath (ORS), an inner root sheath (IRS), and a hairs haft (HS). The lower part of the follicle, the hair bulb, is characterized by proliferating matrix cells (M) and by the dermal papilla (DP), which is the dermal component of the HF. The major keratins expressed in different compartments are indicated.

Terminal differentiation within the interfollicular epidermis ultimately leads to the formation of a functional skin barrier that protects organisms from water loss, infections, and various insults. During the whole process, distinct signalling patterns specify different developmental stages and these stage-specifically regulated signalling events ensure the correct morphogenesis of skin epidermis and its appendages [72, 74].

Hair follicles (HF) and sebaceous glands, two epidermal appendages, are embedded in the dermis and are separated from the dermis by the basement membrane, whose components are secreted by epidermal keratinocytes and dermal fibroblasts. The epidermal stem cell compartment resides in the basal layer of the epidermis and in a specific region of the outer root sheath, named *bulge*.

Specialized cells of the epidermis include melanocytes, which produce the pigment melanin, and Langerhans cells, which are the main skin-resident immune cell. In addition, T cells, mainly CD8+ T cells, can be found in the stratum basale and stratum spinosum [75].

The skin is a well-recognized target of thyroid hormone, which is an important regulator of epidermal homeostasis [76]. The effects of TH on keratinocyte dynamics are mostly exerted through transcriptional regulation mediated by the genomic action of the two TH nuclear receptors, TRα and TRβ, which act both as positive or negative regulators of transcription on different promoters and in different pathophysiological conditions [77].

A striking example is given by the amphibian metamorphosis, when TH governs various differentiation programs comprising the switch from a bilayer non-keratinized epithelium into a stratified, keratinized epidermis [78].

Especially, TH in skin exerts profound effects on fetal epidermal differentiation, barrier formation, hair growth, wound healing, keratinocyte proliferation, and keratin gene expression [79].

Indeed, TH action is crucial for the balance between proliferation and differentiation in normal and pathological conditions, including epidermal regeneration [80] and cutaneous cancer [81].

Many keratins have been identified as TH-responsive genes [82]. In amphibian metamorphosis, TH is required for skin changes and correlates with the expression of adult keratins and the loss of embryonic keratins [83]. In mammalian epidermis and in the HF, TH regulates a number of keratins, including K5, K14, K6, K16, and K17 [80,

84-87]. Similarly, TRα and TRβ can regulate either positively or negatively the expression of selected keratins in cultured cells [82, 88-90].

In humans, thyroid dysfunction is associated with alterations in skin architecture and homeostasis [91]. Hyperthyroidism in humans leads to alterations in the skin homeostasis and increases perspiration, heat, pruritus, itching, urticaria, vitiligo, and enhanced pigmentation. In addition, the epidermis is usually thinner than normal [92].

In hypothyroid subjects, the skin is dry, cold, and rough. The epidermis is hyperkeratotic, alopecia may develop, and there is diffuse myxedema [92].

The concept that a finely tuned TH concentration is essential in the control of proliferation versus differentiation raises the possibility of interfering with such mechanisms for therapeutic purposes.

2.6 Type 3 deiodinase and cancer

The Dio3 gene is localized in the imprinted Dlk-Dio3 region of human chromosome 14 and mouse chromosome 12 and is expressed predominantly by the paternal allele [93].
The human and mouse Dio3 genes have various unique features:
1) they are devoid of introns; 2) they contain a UGA codon located in the open reading frame and a stem-loop mRNA structure (SECIS) in the 3'-UTR of the mRNA that is essential for selenocysteine (Sec) incorporation at the UGA codon [94] and 3) the Dio3 locus contains an overlapping, long-non-coding antisense-transcript (lncRNA) named Dio3-os, which is a common feature of various imprinted genes [95].
In vertebrates, D3 is highly expressed during development and, although its expression decreases in most tissues in adult life, it persists in few organs, as brain, skin, placenta, pregnant uterus and pancreatic b-cells [96-98].
Being the principal physiological inactivator of TH, D3's main function is to protect tissues from an excess of active hormone. Thyroid hormone excess is among the more potent inducers of D3. It represents a homeostatic negative feedback loop by which TH accelerates its D3-mediated degradation. The widespread D3 expression during development in different species and its dynamic and coordinated expression with the TH-activating enzyme D2, reflects the critical importance of the strict regulation of TH levels during development [99].
In mammals, D3 expression at maternal-fetal interfaces is required to constitute a barrier to the maternal-to-fetal transfer of T4, thus maintaining the relatively low TH levels in the fetus since embryonic exposure to excessive levels of maternal TH was found to be highly detrimental [100], while its expression in endometrium suggests that local regulation of thyroid status is important in implantation [81, 98, 100].
The TH inactivation pathway via D3 has recently been implicated in the post-embryonic regulation of proliferation in a number of cell types including keratinocytes and brown adipocyte precursors [81, 101].
Indeed, D3-mediated local hypothyroidism promotes cellular proliferation by regulating the nuclear T3 availability.
Of note, several studies have revealed the re-expression of D3 in different pathophysiological conditions associated with enhanced proliferation, as cardiac

hypertrophy, myocardial infarction (MI), chronic inflammation, critical illness and including cancer [48].

Given its activity in regulating several cell functions, it is not surprising that TH has been involved in the formation and maintenance of neoplastic processes [67].

This finding suggests a link between deiodinase-mediated TH metabolism and carcinogenesis. Because of its presence in fetal and in malignant tissues, D3 is referred to as an '*oncofetal enzyme*'.

Thyroid hormone metabolism as well as D3 overexpression have been shown to play a major role on the growth of various tumors (for example, colon cancer [102, 103] and basal cell carcinoma (BCC) [81, 104]). Interestingly, a common feature of TH in cancer regulation is that TH establishes a feedback loop with most of the oncogenic signal factors that regulate tumorigenesis, such as the sonic hedgehog [104], WNT [103], bone morphogenetic protein [103], Notch [105], phosphoinositide 3-kinase [106] and RAS pathways [107].

The picture that emerges is that thyroid hormone affects various oncogenic and tumor suppressor pathways that in turn alter the balanced expression of Dio2 and/or Dio3, thus resulting in a fine circular loop that amplifies or attenuates tumor growth[103, 104].

BCCs are clear-cut examples of how DIO3-induced attenuation of thyroid hormone signalling promotes and sustains cancer cell proliferation and progression (Figure 10) [81, 102, 108].

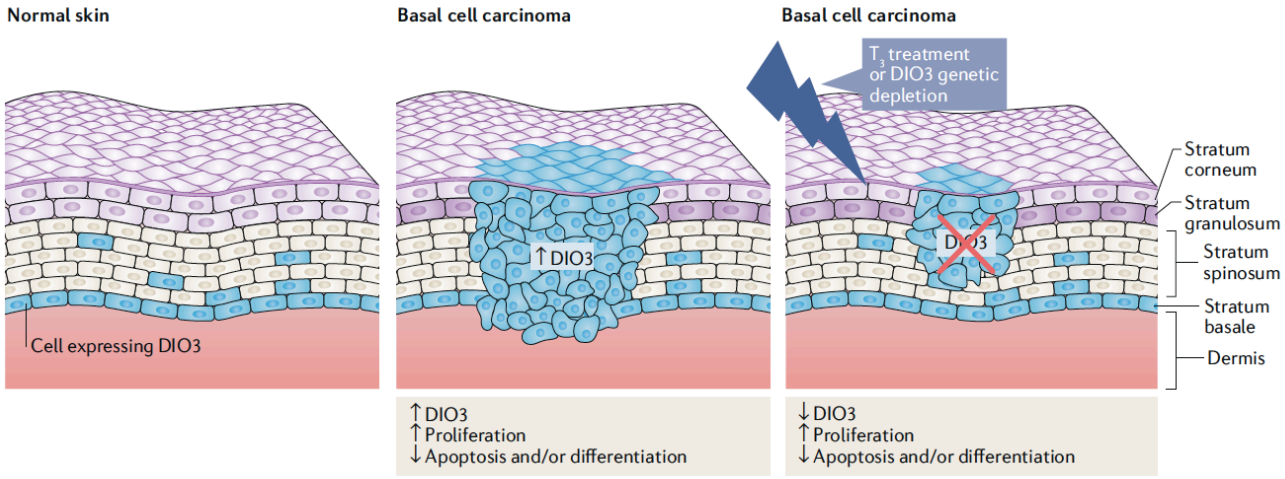

Figure 10

The tumorigenesis of basal cell carcinoma is highly sensitive to thyroid hormone action.

DIO3 is expressed in the basal layers of normal skin and its expression gradually decreases in the upper layers. In many tumorigenic contexts, particularly in basal cell carcinoma (BCC) tumours, DIO3 expression is potently upregulated. In BCC tumours, DIO3 inactivates thyroid hormones and enhances proliferation of BCC cells. Depletion of DIO3 or thyroid hormone treatment with liothyronine drastically reduces BCC growth by inducing BCC cell apoptosis.

Proliferation and survival of BCC cells is physiologically regulated by the Hedgehog (Hh) pathway, which plays a pivotal role in embryogenic development and tumorigenesis [109-112].

Vertebrates possess 3 Hedgehog (Hh) proteins, Sonic Hh (Shh), Indian hedgehog (Ihh), and Desert hedgehog, all of which bind to the receptor patched homolog (Ptch)-1. Upon Hh binding, the signal is transduced to the ultimate effectors of the pathway, namely, the zinc-finger transcription factors glioma associated oncogene Gli1, Gli2, and Gli3 [104]. Aberrant activation of the Hh signalling pathway is involved in several malignancies, and the signalling pathway is inappropriately activated in up to 25% of human tumors [113]. Proliferative effects have been associated with activation of the Hh pathway in several systems [114, 115]. In skin, constitutively active Shh signalling causes formation of hair follicle-derived tumors, of which BCC represents the most common cancer in humans [113, 116]. Mutations in the patched receptor (PTCH), which is an inhibitory component of the Hh pathway, have been identified in patients with Gorlin's syndrome [117, 118] that is associated with high rates of BCC and medulloblastoma. Besides misexpression of Hh molecules, ligand-independent signaling, such as amplification of Gli1 or Gli2, mutations in PTCH or Smoothened (SMO), are correlated with several types of human cancers [119, 120].

Therapeutics strategies targeting Sonic hedgehog (Shh) signalling are currently used in different clinical trials for the treatment of cancer patients and represent an important nonsurgical approach to interfere with BCC occurrence and growth [121]. D3 is overexpressed in BCCs of both mouse and human origin, and is under the control of Shh, which increases Dio3 expression by acting via a conserved Gli2 binding site on the human Dio3 promoter [81]. By decreasing TH action in the BCC microenvironment, D3 promotes BCC tumorigenesis. In addition, Gli2 and the Shh pathway are negative targets of TH, which thus attenuates cancer formation [104].

Interestingly, a recent study of my group has shed light on a reciprocal regulation between TH action and the cancer-associated microRNA-21 (miR21) in basal cell carcinoma (BCC) skin tumors [122]. miR21 has been related to the pathogenesis of various malignant tumors, including prostate, gastric, colon, breast, and lung cancer [47, 113-120, 123].

Apart from being involved in carcinogenesis, miR21 plays a crucial role in a plethora of biological functions and diseases, namely development, cardiovascular diseases, and inflammation [124]. miR21 is also expressed in skin [125-127], and its potential role as a regulator of skin homeostasis is demonstrated by its upregulation in such diseases as psoriasis, atopic dermatitis [128, 129], melanoma, and squamous cell carcinoma (SCC) [130-132].

Interestingly, miR21 is a negative TH target and also modulates TH metabolism by inducing D3 expression. Moreover, a new miR21 target gene, GRHL3 (Grainyhead Like Transcription Factor 3), which is a transcription factor expressed in the skin essential for keratinocyte differentiation [133-136], is a novel suppressor of D3 and accounts for the positive regulation of miR21 on D3 levels (Figure 11).

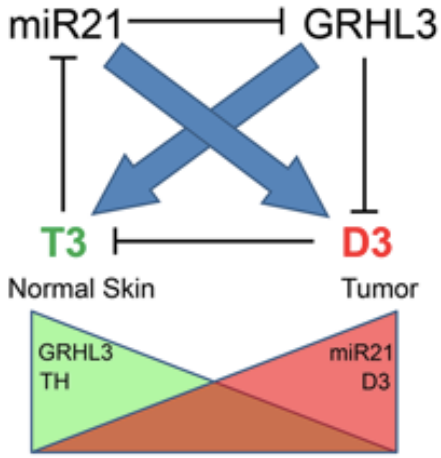

Figure 11

BCC tumorigenesis requires an intact miR21/GRHL3/D3 axis.

Schematic representation of the mutual, negative-feedback loop by which TH regulates miR21 and miR21 controls intracellular TH through GRHL3.

These data demonstrate the existence of a miR21/GRHL3/D3 regulatory circuit that leads to a reduction of the TH signal in the tumor microenvironment. Disruption of this regulation in vivo drastically attenuates the oncogenic potential of BCC cells [122].

Importantly, genetic skin specific Dio3 depletion in a mouse model with spontaneously forming BCC tumors, drastically reduces tumor occurrence and prevents miR21 overexpression in these tumors.

Therefore, TH functions as a suppressor of BCC tumors by regulating multiple pathways, irrespective of miR21, and identify the TH-inactivating enzyme D3 as a potential target of anticancer therapy able to attenuate BCC growth [81, 122].

Although D3 is the deiodinase most involved in cancer formation, my group recently found that also the type 2 deiodinase, D2, is expressed in tumor cells and in BCC [108]. The expression of both, D2 and D3 in BCC suggests that their action fine-tunes the TH signal in this cellular context. Indeed, we observed that manipulation of D2 or D3 dramatically affects the proliferative potential of BCC cells [108]. These results are compatible with the recent finding that precise regulation of the TH-dependent landscape of gene expression is essential in a vast range of biological processes, namely, embryonic development, tissue repair, and tumorigenesis [66].

From a broad perspective, these novel concepts expand the use of deiodinases as a tool with which to interfere in diverse pathophysiological contexts in order to adapt the TH signal in a tissue-specific fashion.

3. Aim of the project

Thyroid hormones (TH) T3 and T4 regulate the metabolism and growth of all cell types, and thus strongly impact on cancer [48]. Intracellular TH signaling is adapted within target cells via the action of the deiodinase enzymes D2 and D3. In detail, D2 confers on cells the capacity to produce extra amounts of T3 thereby enhancing TH signaling, whereas D3 has the opposite effect [66].

The deiodinase system is often altered in such pathological conditions as cancer. In fact, the type III deiodinase (D3), rarely expressed in adult life, results re-activated in various types of human cancers where plays a critical role in the regulation of cell proliferation.

Several studies have demonstrated that D3 is overexpressed also in Basal Cell Carcinoma (BCC), the most frequent skin cancer and that this event is under the control of the Shh pathway [81]. Attenuation of TH by D3 in BCC cells is sufficient to enhance susceptibility to cancer formation [81].

The anti-tumorigenic action of TH in BCC can be attributed to its ability to reduce tumor cell proliferation, and increase the apoptotic rate [108, 137]. Accordingly, TH treatment reduces tumor growth by attenuating the oncogenic potential of the BCC tumor drivers Shh and miR21 [104, 122].

Is D3 expression limited to BCC or do other skin tumoral lesions express D3?

However, how TH impacts on the progression, invasiveness and metastasis of skin cancers is largely unknown.

My PhD project aimed to understand the effects of TH signaling and D3 overexpression in a different model of skin cancer, the SCC, which provides a better model to assess the role of TH metabolism not only in a context of relative benign tumorigenesis, but also to evaluate during the different stages of the neoplastic process.

Since BCCs are benign and not prone to progress, we studied the more aggressive Squamous Cell Carcinoma (SCC) tumors. In detail, we investigated how type III deiodinase is regulated during cSCC progression and evaluated whether and how perturbation of the deiodinase-driven regulation of TH metabolism functionally impacts on the behavior of cSCC.

4. Results

4.1 TH signalling is dynamically regulated during tumorigenesis.

To investigate the role of TH and its metabolism in the progression, invasiveness, and metastasis of skin cancers, we studied the expression of D2 and D3 in different stages of SCC using the two-step chemically induced carcinogenesis model [138]. In the first, initiation step, mice were treated with the mutagen DMBA; in the second promoting step, mice were treated with 12-O-tetradecanoyl-phorbol-13-acetate (TPA), a drug that stimulates epidermal proliferation and inflammation (Fig. 12A). Because of the lack of functional D2 antibodies in commerce, carcinogenesis experiments were performed in the knock-in D2-Flag mouse [139] in which the endogenous Dio2 gene is fused to the Flag tag. As shown in Figure 12B, D3 rapidly increased during the initial tumorigenic step and peaked at the hyperplastic epidermis stage. D3 was highly expressed up to the formation of papillomas, which are benign intermediate lesions in the multistage progression to skin carcinoma [140] (Fig. 12B). D2 expression began at later time points and reached a nadir at the final phases of tumorigenesis when papillomas lose their differentiation potential, become more invasive and turn into SCCs (Figure 12B, C). D2 was closely associated with the expression of K8, which is a simple epithelial keratin absent in normal epidermis but often detected in advanced SCCs [141]. mRNA analysis confirmed the sequential expression of D3 and D2 at 15 and 30 weeks after DMBA/TPA treatment (Fig. 12C). Notably, the dynamic expression of D2 and D3 is consistent with lower intra-tumoral T3 levels in the papillomas then in the more advanced SCCs (Fig. 12D). Co-expression of D2 and D3 with markers of specific stages of tumorigenesis was confirmed by western blot and immunofluorescence analysis (Fig. 12B, E and F). In detail, D2 expression was associated with reduced E-cadherin and enhanced vimentin expression, which is a sign of the EMT typical of advanced SCCs (Fig. 12F).

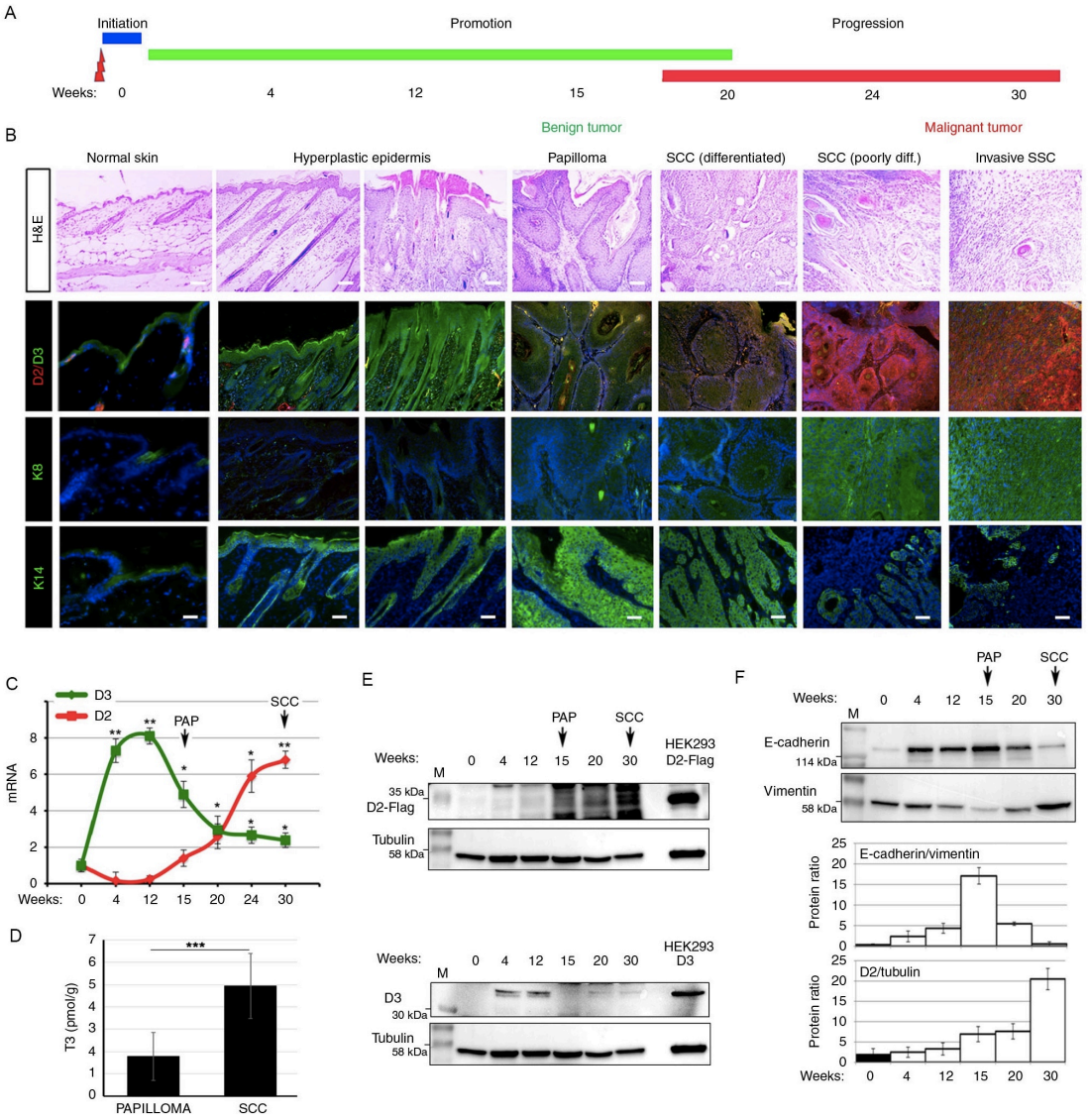

Figure 12

D2 and D3 are dynamically expressed during SCC tumor initiation and progression.

(A) Schematic representation of the two-step carcinogenesis experiment. **(B)** Representative H&E, D2/D3 co-staining, and K8 and K14 staining of DMBA-TPA-treated skins for the indicated weeks. Images represent tumors of one of eight different D2-Flag mice analyzed for each time point ($n = 8$). Scale bar represents 200 µm. **(C)** mRNA levels of D2 and D3 were measured in progressive DMBA-TPA-treated skins as indicated in **a** and **b**, by real-time PCR analysis ($n = 8$). **(D)** Intracellular T3 was measured as indicated in the "Methods" section in dorsal skin tissues from mice treated with DMBA-TPA for 15 (PAP) and 30 (SCC). **(E)** Western blot analysis of D2-Flag and D3 expression from skin lesions of D2-3xFlag mice treated with DMBA-TPA for the indicated times ($n = 8$). HEK293 cells transfected with D2-Flag or D3 served as D2 and D3 controls, respectively. Arrows indicate the papillomas (PAP) and SCC tumors. **(F)** Western blot analysis of E-cadherin, vimentin, and tubulin in the same samples as in **e**. Quantification of the single protein levels versus tubulin levels and the E-cadherin/vimentin ratio is represented by histograms.

Thus, our results show that the EMT of SCC coincides with a switch in D3- D2 deiodinases. Indeed, while D3 is a marker of the initial stages of tumorigenesis, D2 expression is associated with cancer progression.

4.2 Sustained TH signaling accelerates tumor invasion

To gain insight into the role of TH during the early stage of chemical tumorigenesis, we disrupted the TH signal by depleting D3 in the epidermal compartment. To this end, we crossed the $D3^{fl/fl}$ [142] mice with the $K14Cre^{ERT}$ mice [143], thus generating the $K14Cre^{ERT+/-}$, $D3^{fl/fl}$ (skin D3KO, sD3KO) and $K14Cre^{ERT-/-}$, $D3^{fl/fl}$ (CTR) mice. D3 wad depleted by tamoxifen treatment, and DMBA/TPA was applied to the dorsal skin one week later (Figure 14 A). Effective D3-depletion from the epidermal compartment was confirmed by PCR and immunofluorescence (Figure 13 A, B).

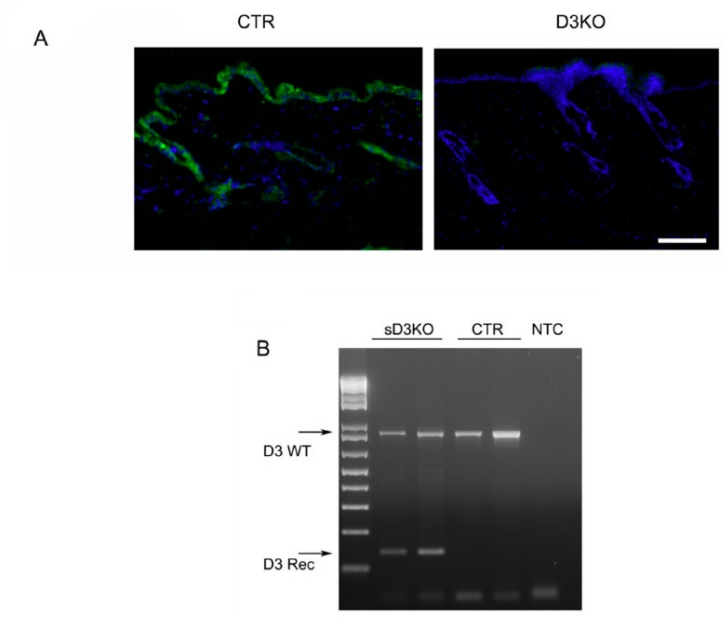

Figure 13

D3-depletion in the epidermal compartment.

(A) D3 depletion in sD3KO mice was confirmed by immunofluorescence analysis of dorsal skin of sD3KO and control mice. Scale bars represented 100 μm. (B) D3 depletion in sD3KO mice was confirmed by PCR analysis of the same dorsal skin as in A.

Dorsal skin and skin lesions were collected 8 and 15 weeks after treatment. Eight weeks after DMBA treatment, the analysis of skin morphology and of the markers of epidermal hyperplasia, i.e., K14 and K6, showed that tumor formation was much lower in sD3KO mice than in controls (Figure 14 B). Accordingly, tumor formation was attenuated in sD3KO mice 15 weeks after DMBA treatment. D3-depletion reduced the frequency (number of tumors at each time point) and the incidence (time of lesion appearance) of cancers (Figure 14 C).

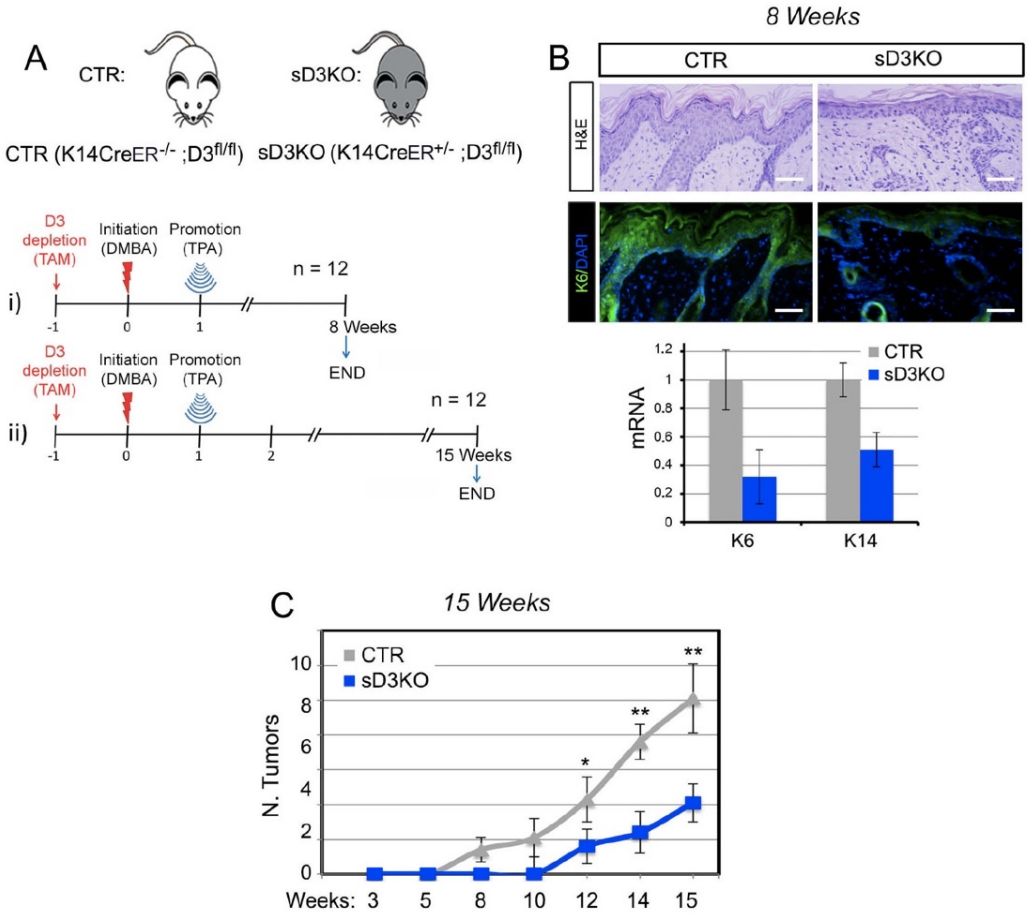

Figure 14

Increased thyroid hormone action in epidermal-specific D3KO mice reduced the frequency and incidence of SCC tumor formation.

(A) Schematic representation of D3-depletion and the two-step carcinogenesis experiment in 12 CTR and 12 sD3KO samples (n = 12). b Representative H&E and K6 staining of DMBA-TPA-treated CTR (n = 8) and sD3KO (n = 8) skins for 8 weeks. Scale bar represents 200 μm (top). mRNA levels of K6 and K14 were measured by real-time PCR analysis in 16 lesions from CTR mice and 16 lesions from sD3KO mice (bottom). (C) The number of skin lesions was counted during the two-step carcinogenesis experiment as indicated in A (ii). Tumor incidence is expressed as the number of tumors per mouse.

Strikingly, based on morphological features, the few skin lesions observed in the sD3KO mice were more advanced lesions then those in control mice (Figure 15 A). Accordingly, K8 expression was higher in D3KO mice than in control mice, which suggests that D3-depletion accelerates SCC formation (Figure 15B). The E-cadherin/N-cadherin ratio was lower in D3KO lesions than in control lesions, which confirms the more advanced stage of these lesions in D3KO mice (Figure 15 C, D). These results indicate that TH plays an unexpected stage-specific role in SCC development, i.e., T3 slows the early stages of tumorigenesis, but induces SCC progression (Figure 15 E).

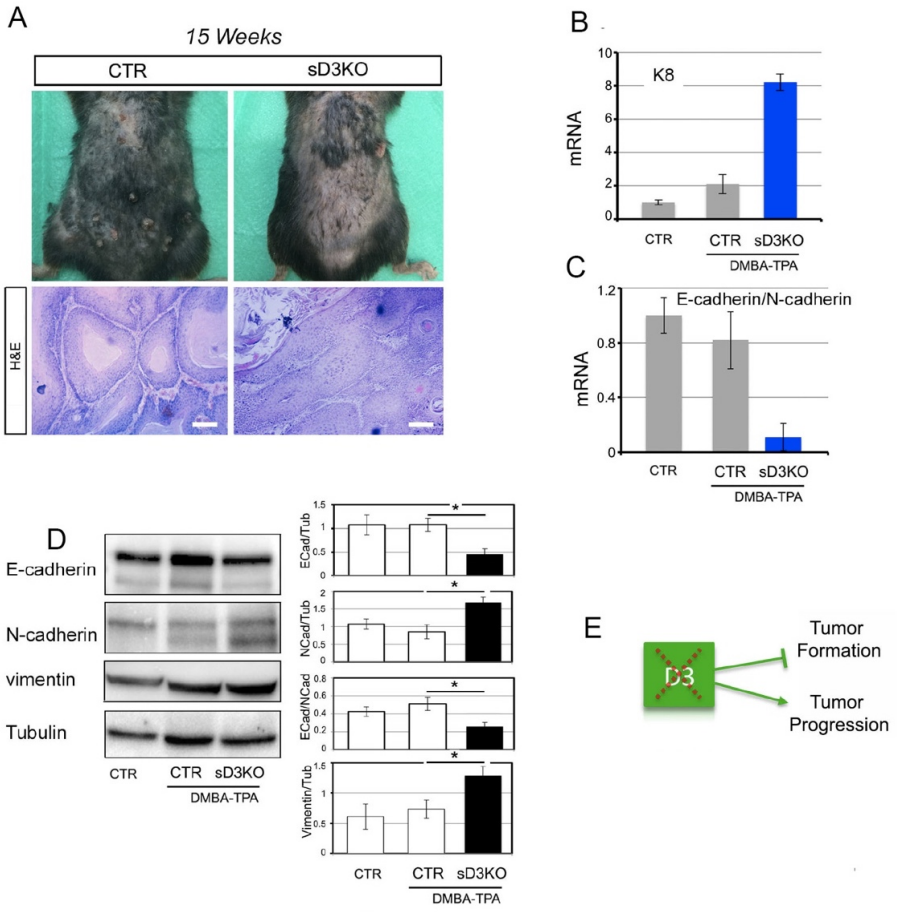

Figure 15

Increased thyroid hormone action in epidermal-specific D3KO mice enhanced the migration and invasion potential of SCC. (A) Representative images of the dorsal skin from CTR and sD3KO mice treated with DMBA-TPA for 15 weeks (n = 12). H&E of the skin lesions from CTR (n = 6) and sD3KO (n = 6) mice treated with DMBA-TPA for 15 weeks. Scale bar represents 200 µm. (B) mRNA levels of K8 in the dorsal skin of CTR (n = 15) and sD3KO (n =15) mice. (C) mRNA levels of E-cadherin/N-cadherin in skin lesions of CTR (n = 15) and sD3KO (n = 15) mice measured by real-time PCR analysis. (D) Western blot analysis of E-cadherin, N-cadherin, and vimentin expression in skin lesions of CTR (n = 10) and sD3KO mice (n = 10). Quantification of the single protein levels versus tubulin levels and the E-cadherin/N-cadherin ratio is represented by histograms. *P< 0.05, **P< 0.01. (E) Schematic representation of the effects of D3-depletion on SCC tumor growth and progression.

4.3 Intracellular T3 induces Epithelial-Mesenchymal Transition (EMT) of SCC cells.

Given the effects of D3-depletion in SCC progression, we investigated whether the TH signal is a positive regulator of the invasive conversion of cancer cells. Consequently, we evaluated the contribution of the TH signal to the promotion of the Epithelial-mesenchymal transition (EMT) in the human skin squamous cell carcinoma SCC 13 cells. As shown in Figure 16 A, T3 treatment increased N-cadherin expression and slightly reduced E-cadherin expression, thereby resulting in a net attenuation of the E-cadherin/N-cadherin ratio, which indicates an increased EMT profile. We also measured the expression of two other EMT markers namely, vimentin and Twist, and found that both were positively regulated by T3 (Figure 16 B). These results were confirmed in two other SCC cell lines (the head and neck SCC cells SCC 011 and SCC 022). Indeed, T3 treatment reduced the E-cadherin/N-cadherin mRNA ratio and increased the mRNA expression of vimentin and Twist (Figures 16 C, D, E).

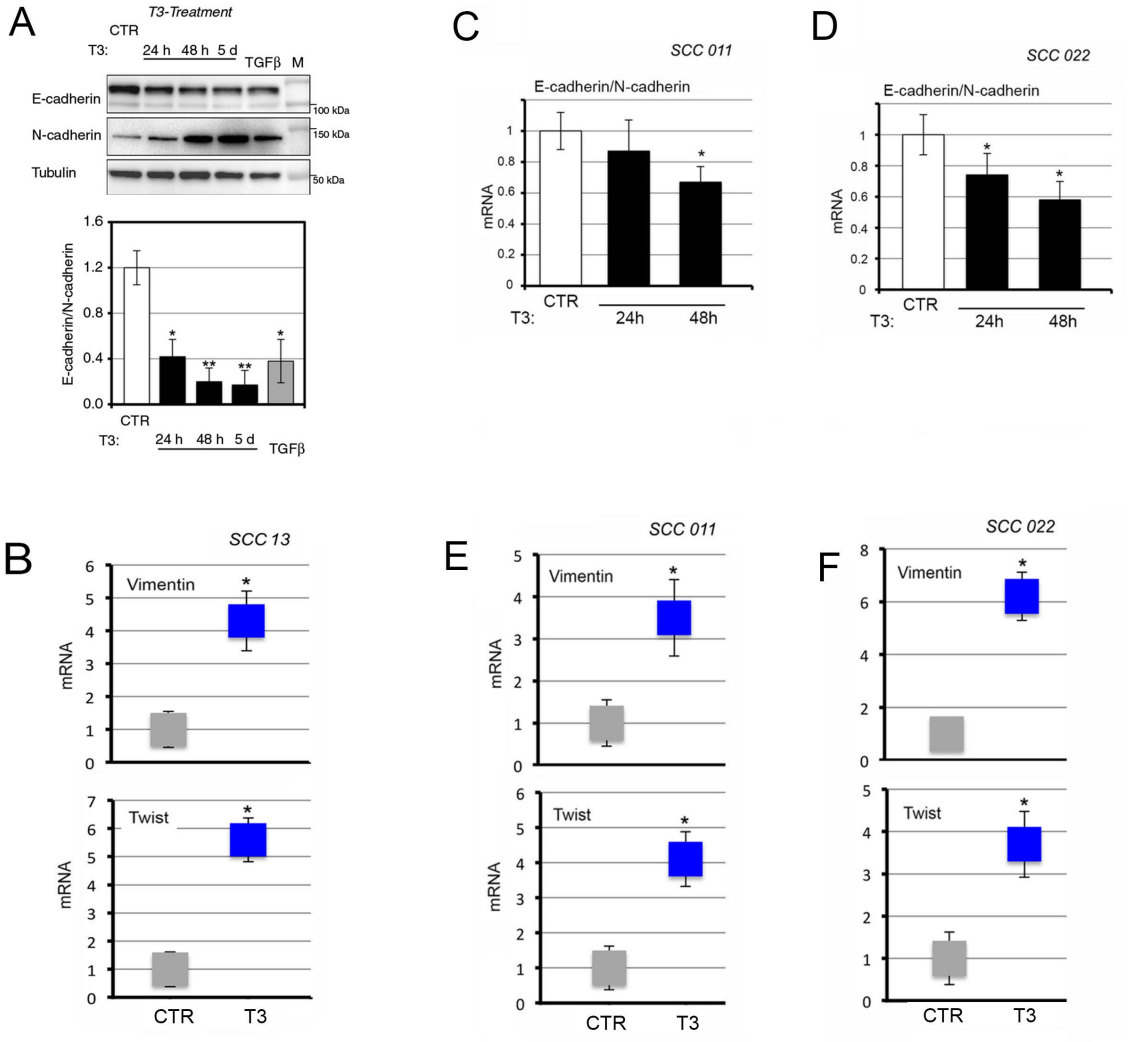

Figure 16

Thyroid hormone activation induces the epithelial–mesenchymal transition of SCC13 cells.

(A) SCC cells were treated with 30 nM T3 for different time points or with 5 ng/µl TGFβ for 48 h. Total protein lysates were used for western blot analysis of E-cadherin and N- cadherin expressions. Tubulin expression was measured as loading control. One representative immunoblot of seven is shown (top). Quantification of the E-cadherin/N-cadherin ratio in the western blot is represented by histograms. (B) Vimentin and Twist mRNA expression in SCC13 cells treated with 30 nM of T3 for 48h. (C-D) E-cadherin/N-cadherin mRNA expression and their ratio were measured by Real Time PCR in SCC011 and SCC022 cells treated with 30 nM of T3 for 24 e 48h. (E-F) Vimentin and Twist mRNA expression in SCC011 e SCC022 cells treated with 30 nM of T3 for 48h.

To explore the role of the intracellular control of TH action in EMT, we suppressed D2 or D3 expression in SCC 13 cells using CRISPR/Cas9 technology. D2-depletion and D3-depletion were verified by gene sequencing and PCR analysis (Figure 17 A-B). Western blot revealed that D3-depletion (which increases intracellular T3) phenocopied the effects exerted by T3 on the EMT. Indeed, the E-cadherin/N- cadherin ratio at mRNA and protein level was reduced in D3KO cells and in T3-treated cells (Figures 17 B, C). Accordingly, the E-cadherin/N-cadherin ratio was elevated in

D2KO cells versus control cells (Figure 17 E). The expression of the EMT markers vimentin and Twist was also inversely regulated in D2KO cells versus D3KO cells (Figure 17 E).

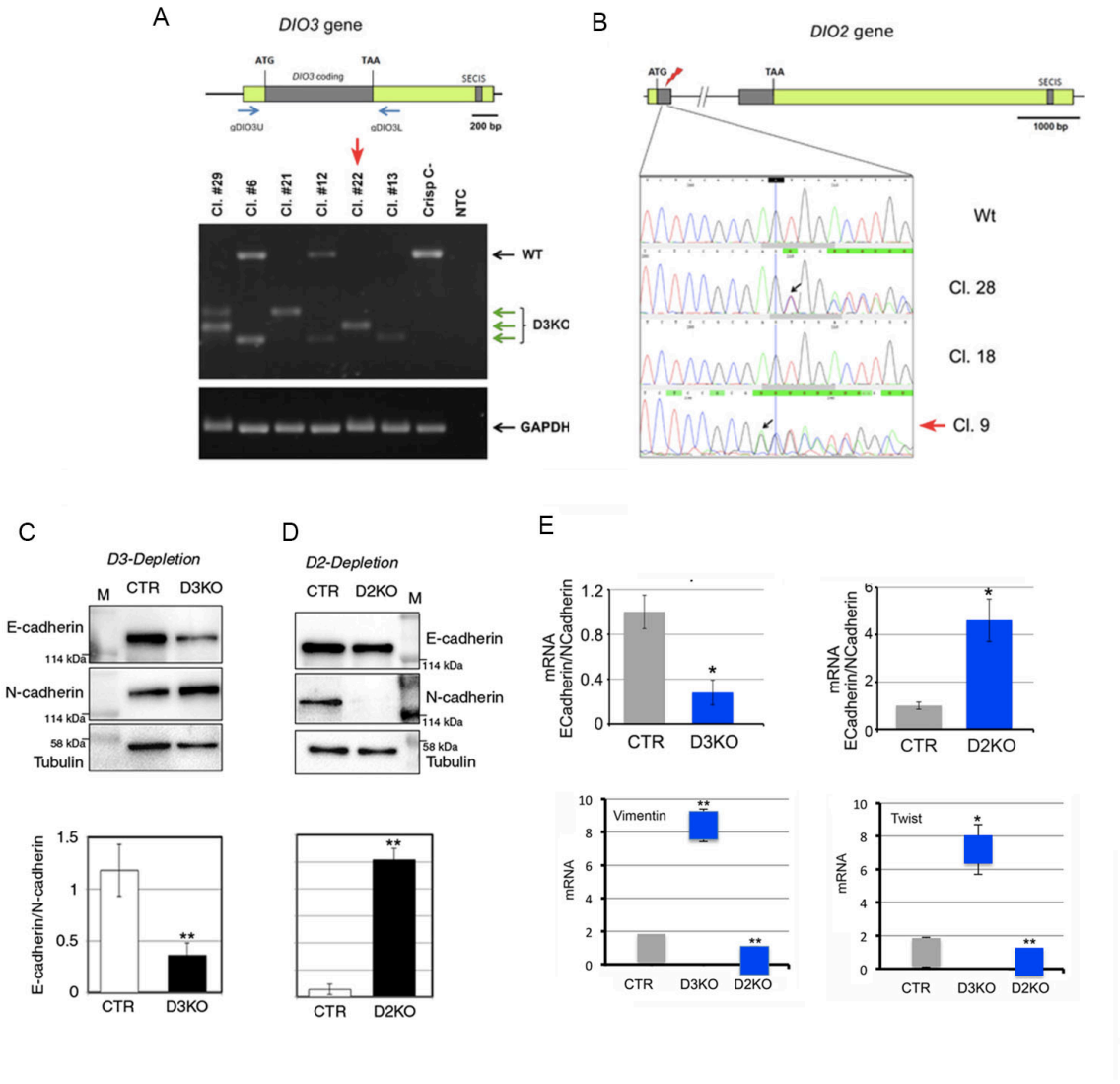

Figure 17

Markers of EMT are inversely regulated in D2KO cells versus D3KO cells.

(A) Schematic representation of Dio3 locus; mutagenesis of Dio3 was assessed by PCR analysis. The green arrows indicate the mutated DIO3 products. (B) Schematic representation of Dio2 locus; mutagenesis of Dio2 was assessed by genomic DNA sequencing of exon 1. (C) Western blot analysis of E-cadherin and N-cadherin expressions in SCC-D3KO cells. (D) Western blot analysis of E-cadherin and N-cadherin expressions in SCC-D2KO cells. (E) E-Cadherin/N-Cadherin ratio, Vimentin and Twist mRNA expression level was evaluated by Real Time PCR in D3KO cells and in D2KO cells compared to the control, CRISP-CTR SCC cells.

However, D3-depletion and T3 treatment of SCC cells caused a morphological shift, namely, delocalization of phalloidin from the membrane to the cytoskeleton, an increase of vimentin expression and a decrease of E-cadherin expression (Figure 18 A, B).

Notably, T3 reduced SCC cells proliferation (Figure 18 C), which confirms its effects as an anti-proliferative agent in SCC, but contextually, it enhanced the migration of SCC cells (Figure 18 D). Accordingly, D3-depletion in D3KO cells caused growth attenuation, but enhanced migration (Figure 18 E, G), whereas D2KO cells had the opposite profile, increased proliferation and reduced migration (Figure 18 F, G).

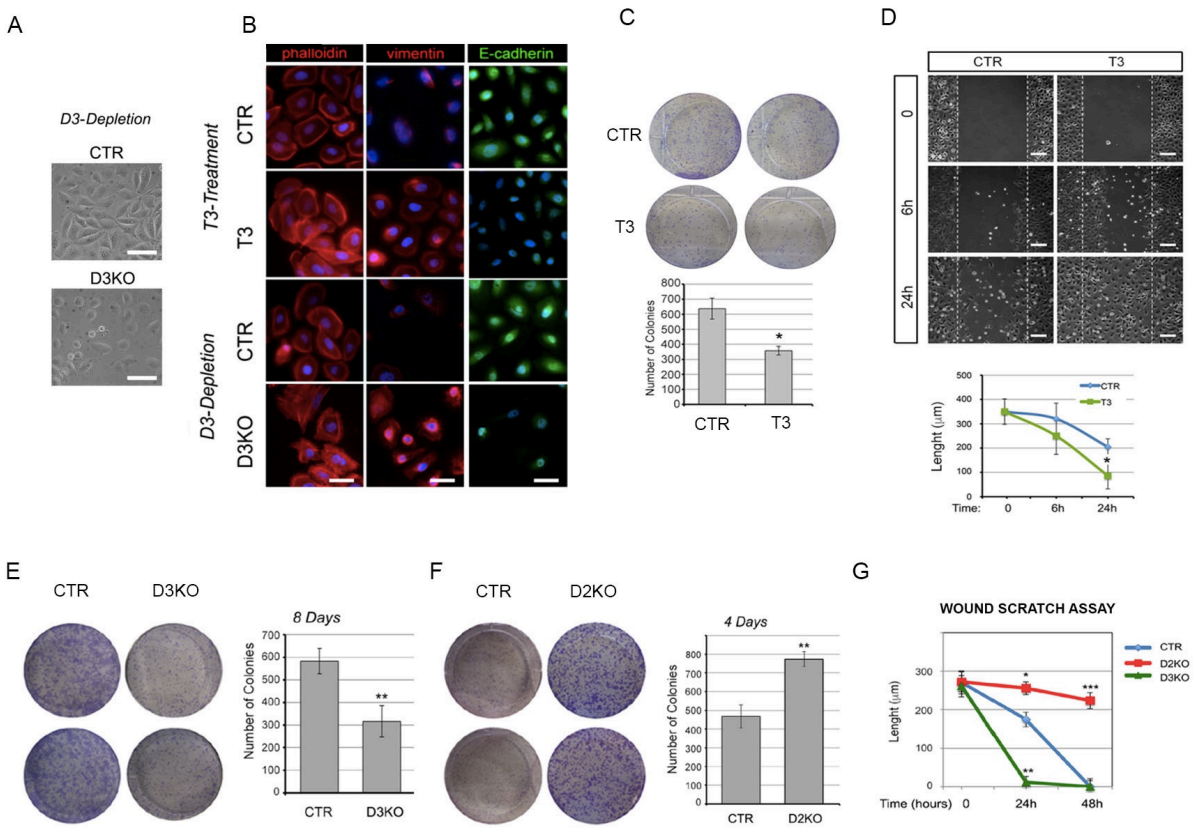

Figure 18

Thyroid hormone activation induces the epithelial–mesenchymal transition and migration and invasion ability of SCC cells. (A) Representative phase contrast of CTR and D3KO cells. Scale bars represent 50 µm. (B) Phalloidin (red), Vimentin (red), and E-cadherin staining (green) of untreated and T3-treated SCC cells, SCC-CTR cells, and SCC-D3KO cells. One representative experiment of 5 is shown. Scale bars represent 50 µm. *P < 0.05, **P < 0.01. (C) Cell proliferation was assessed by colony assay of SCC cells treated or not with 30 nM T3 (top). The number of colonies formed 8 days after plating shown by scale bars (Bottom). One representative assay of five is shown. (D) Wound scratch assay was performed in SCC cells after treatment with T3 (30 nM) for 0, 6, and 24 h. Cell migration was measured as described in the "Methods" section. Scale bars represent 200 µm. (E) Clonogenic assay of CTR and D3KO cells; representative images of petri dishes are shown. (F) Clonogenic assay of CTR and D2KO cells; representative images of petri dishes are shown. (G) Wound scratch assay was performed in in D3KO cells and in D2KO cells compared to the control, CRISP-CTR SCC cells.

To assess whether T3 induced invasiveness as well as migration, we performed a transwell invasion assay and found that T3 significantly increased the invasiveness of SCC cells (Figure 19 A), and, similarly, D3KO cells invaded the matrix more efficiently than did control cells (Figure 19 B).

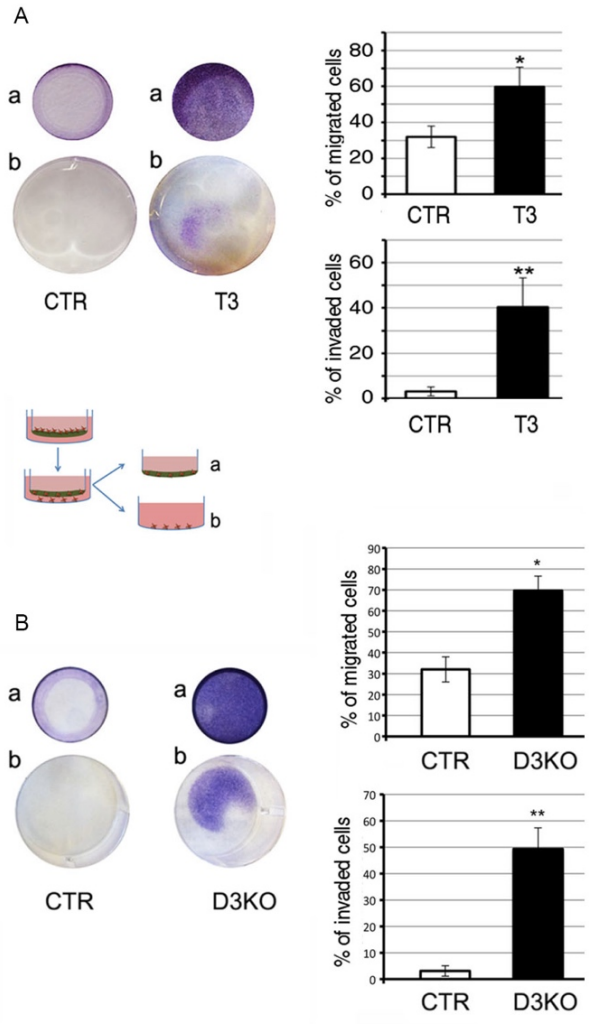

Figure 19

Thyroid hormone treatment or D3-depletion increases invasiveness of SCC cells.

(A) Invasion assay performed on SCC cells treated or not with 30 nM T3 for 5 days. (**b**) Represents cells that invaded on the receiver plate and the area covered by invaded cells is indicated. The percentage of cells that migrated and invaded are represented by histograms. (B) Invasion assay performed on SCC CTR and D3KO cells. The percentage of cells that migrated and invaded are represented by histograms.

Since T3 induced matrix degradation (Figure 19 A, B), we extended the analysis to metalloproteases, which are important inducers of invasiveness and of the EMT. We analyzed the expression patterns of a panel of seven metalloproteases (MMP 2, 3, 7, 8, 9,

10, and 13) in D3KO and D2KO cells versus control cells. Real-time PCR analysis revealed that the expression of MMP 2, 3, 7, and 13 was higher in D3KO cells and lower in D2KO cells than in controls (Figure 20 A). Accordingly, secretion in the culture medium and the enzymatic activity of metalloproteases 2, 3, 7, and 13 were robustly increased in D3KO and reduced in D2KO cells (Figure 20 B, C). These results show that TH acts as an up-stream regulator of cell matrix degradation and of the cell invasion process.

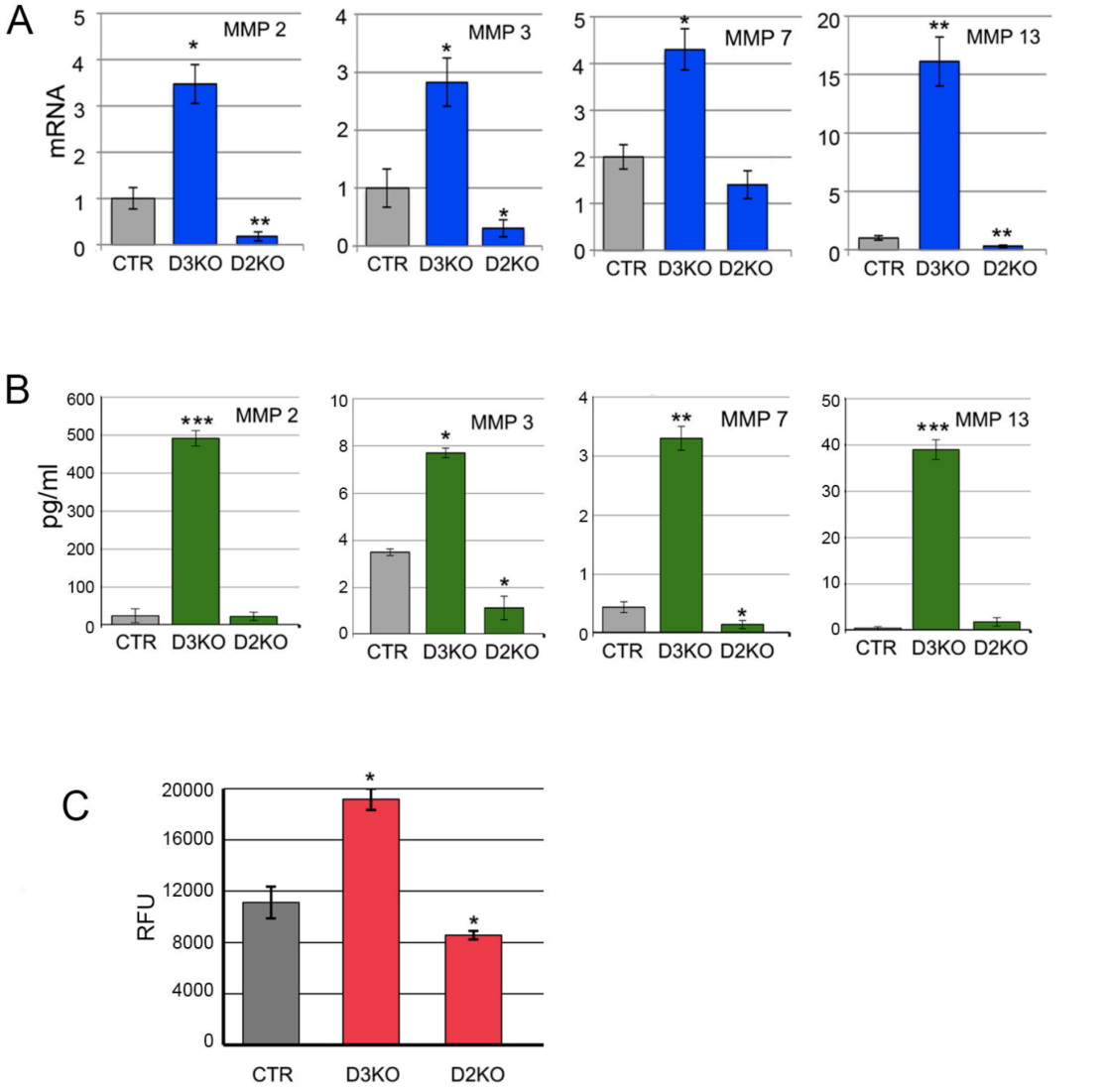

Figure 20

D3 depletion increases the activity of metalloproteases.

(A) Metalloproteases 2, 3, 7 and 13 mRNA expression were analyzed by real time PCR in D3KO, D2KO and CTR cells. (B) Rate of secretion of Metalloproteases was measured in the culture medium. (C) Enzymatic activity of Metalloproteases was measured by Elisa.

4.4 Evidence of a T3-ZEB-1 functional network.

We next investigated the molecular mechanisms by which T3 induces the EMT and invasiveness of SCC cells. We profiled the expression of 84 genes whose expression is related to the EMT using the human EMT RT² Profiler™ PCR Array (Qiagen). Interestingly, most of the EMT genes were modified by D3-depletion (Figure 21 A). In particular, 22 EMT-positive regulators, among which vimentin, N-cadherin, ZEB-1, and Col1a2, were up-regulated in D3KO cells, while 13 genes were down-regulated, among which, the epidermal markers keratin 14 and E-cadherin, which indicates massive induction of the EMT-mediating cascade (Figure 21 B-C). We validated the expression profile of these genes in control and D3KO cells by real-time PCR (Figure 21 D). To identify the EMT genes that mediate TH-dependent invasiveness, we first assessed the possibility that ZEB-1, a prime transcriptional factor in the EMT cascade [144], and an up-stream regulator of many EMT-related genes [145], could be a direct target of TH. Interestingly, in silico analysis of the ZEB-1 promoter region (comprising the 5′-flanking region, 2 kb-up and 2 kb-down the TSS, Figure 22 A) revealed the presence of several thyroid hormone responsive elements (TREs)-binding sites. Chromatin IP (ChIP) confirmed that the thyroid receptor (TRα) physically binds the identified TRE regions (Figure 22 B).

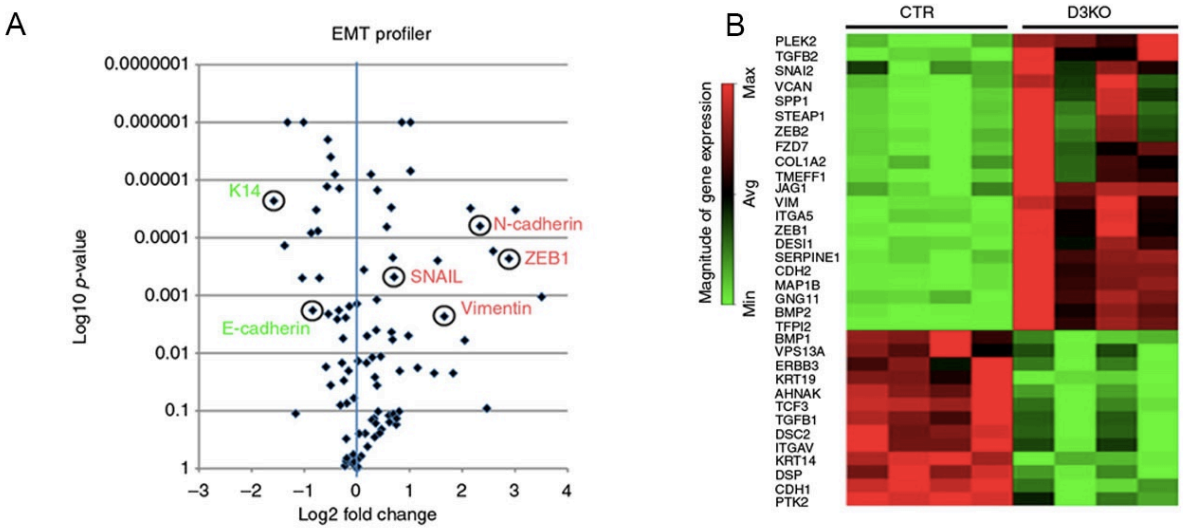

C

Up-regulated genes

Gene	Fold Change	p-Value
MAP1B	8,0556	0,000033
ZEB1	7,3871	0,00023
BMP2	6,0002	0,000171
CDH2	5,0455	0,000063
TFPI2	4,4537	0,000031
VCAN	4,1267	0,006012
SPP1	3,5431	0,022297
TGFB2	2,8879	0,000249
ZEB2	2,7606	0,022277
VIM	2,4368	0,003281
COL1A2	2,2191	0,017992
GNG11	2,0209	0,000001
PLEK2	2,0209	0,000007
JAG1	1,9656	0,005
SERPINE1	1,8025	0,000001
STEAP1	1,7532	0,020452
SNAI2	1,6301	0,000481
TMEFF1	1,5966	0,005836
FZD7	1,5746	0,004339
ITGA5	1,5692	0,00003
DESI1	1,4794	0,000065
CTNNB1	1,366	0,011436

Down-regulated genes

Gene	Fold Change	p-Value
KRT14	0,3345	0,000023
DSP	0,3856	0,000137
KRT19	0,4005	0,000001
AHNAK	0,4863	0,0005
BMP1	0,4948	0,000001
VPS13A	0,5471	0,000083
CDH1	0,5586	0,001817
DSC2	0,5844	0,000033
ERBB3	0,5967	0,000077
TCF3	0,6092	0,000515
ITGAV	0,6736	0,000013
PTK2	0,6807	0,000002
TGFB1	0,6854	0,002131

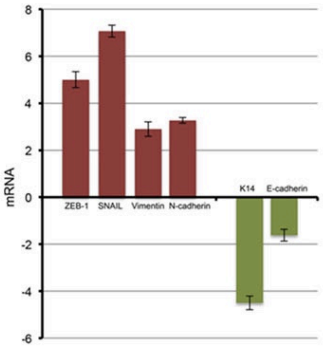

Figure 21

D3 depletion increases the expression of EMT genes.

(A) Vulcano plot of differentially expressed EMT genes measured by real-time PCR in the EMT RT² Profiler™ PCR array (Qiagen). (B) Heat map of gene expression of EMT markers in normal SCC cells versus D3-depleted SCC cells selected by thresholds of p value < 0.05 and log 2-fold changes >1.3 between visits. (C) Expression levels of up- and down-regulated EMT markers in the EMT RT² profiler™ PCR Array. (C) T3-target genes in the EMT RT² profiler™ PCR Array were validated by using Real Time PCR analysis in CTR and D3KO cells.

To assess whether ZEB-1 is a molecular determinant of the T3-dependent EMT, we down-regulated ZEB-1 in SCC cells. Importantly, a scratch assay in SCC cells indicated that ZEB-1 down-regulation (obtained using two different shRNA for ZEB-1 silencing, shZEB-1) completely rescued T3-dependent enhanced migration (Figure 22 C, D). PCR and Western blot analysis of the EMT genes confirmed that ZEB-1 depletion blocks the T3-dependent EMT cascade (Figure 22 E, F). The in vitro and in vivo relevance of the T3-ZEB-1-E cadherin axis was confirmed by measuring ZEB-1 and E-cadherin expression in T3-treated SCC cells or D3-depleted cells compared to control (Figure 22 G, H) and in vivo tumors from DMBA/TPA-treated D3KO mice (Figure 22 I). According to our model, E-cadherin expression was low and ZEB-1 expression was high in sD3KO mice compared to control mice (Figure 22 I).

Taken together, the above-reported results point to a pivotal role of T3 in promoting the EMT in SCC cells, and indicate that T3 induces EMT of SCC cells by promoting Zeb-1 transcription and activating a Zeb-1 dependent EMT program.

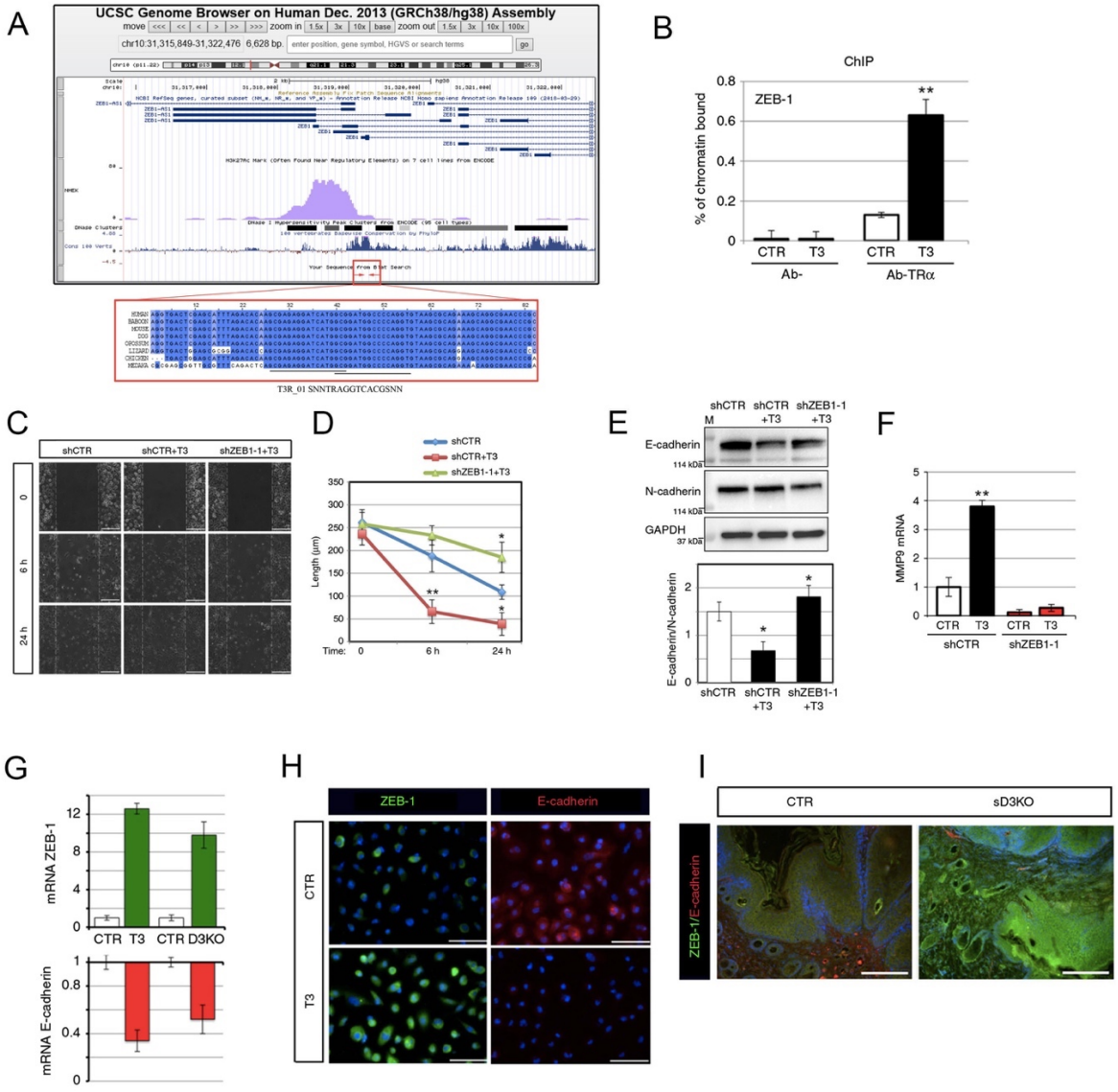

Figure 22

T3 promotes the EMT of SCC by inducing ZEB-1 transcription

(A) Schematic representation of human ZEB-1 5'-Flanking region that contains multiple T3-bindig sites. (B) Chromatin immunoprecipitation (ChIP) of TR binding to the ZEB-1 promoter (region amplified by PCR is indicated by red arrows in A). (C, D) Wound scratch assay of SCC cells after treatment with 30 nM T3 or T3 + ZEB-1 shRNA. Scale bars represent 200 µm. (E) Western blot analysis and the relative quantification of E-cadherin and N-cadherin expressions in SCC cells treated or not with 30 nM T3 and transfected with shCTR or shZEB-1 as indicated. (F) mRNA levels of MMP9 in SCC cells treated or not with 30 nM T3 and transfected with shZEB-1 or shCTR as indicated. (G) mRNA levels of ZEB-1 and E-cadherin in T3-treated versus non-treated cells and in D3KO versus CTR SCC cells. (H) ZEB-1 (green) and E-cadherin staining (red) of untreated and T3-treated SCC cells. One representative experiment of 4 is shown. Scale bars represent 50 µm. (I) ZEB-1 (green) and E-cadherin staining (red) of skin lesions from sD3KO, and CTR mice. One representative experiment of 4 is shown. Scale bars represent 200 µm. *P < 0.05, **P < 0.01.

5. Discussion

Interest in thyroid hormone (TH) in cancer was first aroused by the demonstration, over a century ago, that breast cancer responded to thyroid extract treatment. This suggested that TH is a key regulator of tumorigenesis. However, the role of TH in the whole neoplastic process long remained obscure. The link between TH and cancer was renewed when it became clear that TH receptors and modulators are often altered in cancerous tissues and that modulation of TH might foster cancer cell expansion.

Studies in two different epithelial cancers, namely the basal cell carcinoma and the colon cancer have underlined that the modulation of the intracellular TH levels affects tumor formation, thus prompting interest in tissue-specific TH modulation as an anti-tumoral agent.

Since then a large body of data has accumulated on this topic, pointing to a general mechanism by which TH interferes with oncogenic pathways, thus affecting tumoral formation.

In this study, we demonstrate that during SCC progression a switch occurs in intra-tumoral TH consequent to time-specific action of the TH-inactivating (D3) and TH-activating (D2) enzymes, which affects the behaviour of SCC cells in an *in vivo* model of chemical carcinogenesis.

Our data show that high-TH tumors (D3KO) grow slowly but metastasize rapidly. These conclusions are based on the following results: (1) TH treatment of SCC cells reduced cell proliferation whereas it increased cell migration; (2) TH treatment of SCC cells also accelerated the metastatic conversion of SCC; and lastly, (3) TH-activation (D3KO mice) in vivo attenuated tumor formation but increased invasiveness and the development of metastatic tumors compared with wild-type littermates.

These effects were mediated by a cell-autonomous mechanism of TH activation/inactivation catalysed by the TH-modulating enzymes, D2 and D3, that turn TH on and off in target cells. During chemically induced tumorigenesis, sequential expression of D3 and D2 fine- tunes TH signalling to enable tumor growth during the early stages of tumorigenesis, and invasive transformation at later stages (Figure 12).

Over recent years, our understanding of TH action in cancer has evolved from being a repressor of tumor formation and growth [81, 103, 146] to a factor that induces most of the hallmarks that cancer cells acquire during the later stages of tumorigenesis.

Indeed, our in vitro and in vivo observations demonstrate that while T3 reduced the proliferation of SCC cells, T3 treatment or D3-depletion accelerated cell migration and invasion.

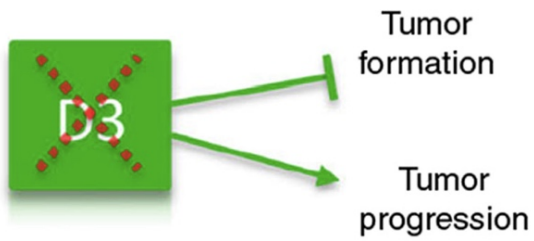

Figure 23

Increased thyroid hormone action by D3-depletion drastically attenuates the growth of a variety of tumor.

Schematic representation of the effects of D3-depletion on SCC tumor growth and progression.

Our finding that D3-depletion reduced SCC formation (Figures 14-15, 23) confirms our previous report that the oncofetal protein D3 is an essential component of the oncogenic route leading to tumor formation. Although D3 is not a canonical oncogene per se and D3 overexpression is not sufficient for tumor initiation, D3-depletion drastically attenuates the growth of a variety of tumors [81, 102, 122].

Furthermore, D3 is positively regulated by the oncogenic pathways Shh [81], miR21 [122], and Wnt [102]. Our data show that, in SCC in vivo, D3 is potently expressed in the early phases of tumorigenesis and its expression coincides with the expression of keratin K6, which is a marker of hyperplastic epidermis (Figures 12, 13). D3 expression declines as tumorigenesis proceeds to more invasive phenotypes. This finding is in line with our previous report that in human colon cancer, D3, which is up-regulated in carcinomas, inversely correlates with the histologic grade of lesions, and decreases as the histologic grade progress from G2 to G3 [102].

How can T3 promote migration and invasion?

For a transformed cell to metastasize to a distant site in the body, it must first lose adhesion, and then penetrate and invade the surrounding extracellular matrix (ECM), enter the vascular system, and adhere to distant organs [147]. We found that TH modulates each of these key steps, and thus facilitates metastatic invasion of secondary sites. Indeed, the increased tumor metastatic conversion induced by T3 was not due to increased tumor cell proliferation but was correlated with (i) increased expression of mesenchymal markers, (ii) condensation of the ECM by MMP proteins,

and (iii) modification of the shape and stiffness of cells.

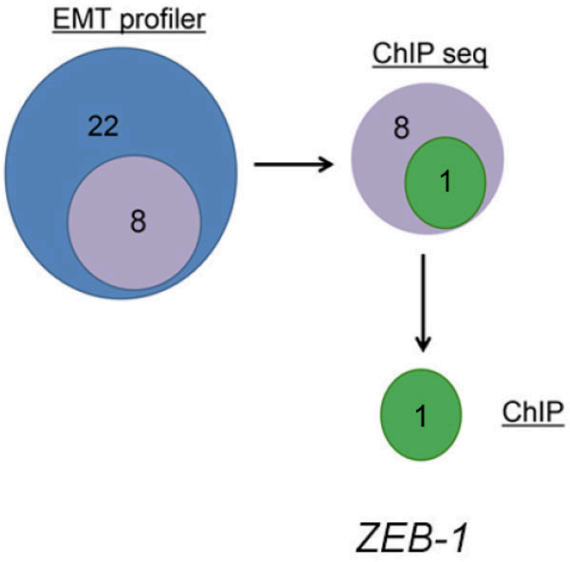

Figure 24

T3 promotes EMT of SCC by inducing ZEB-1 transcription.

Schematic representation of the strategy used to identify the genes regulated by T3 and involved in EMT promotion.

To identify the TH-dependent signature responsible for EMT induction, we used the human EMT RT² Profiler™ PCR array. The TH-positively regulated genes found included the mesenchymal markers vimentin, ZEB-1, Snail, and Col1a2. The negatively regulated genes included the epithelial-specific adhesion molecules K14 and E-cadherin. Chromatin immunoprecipitation assays revealed that among various EMT-related genes, ZEB-1 is physically bound by T3 in SCC cells and that inhibition of ZEB-1 drastically reduced the TH-dependent EMT (Figure 22 C-F). This finding indicates that ZEB-1 is a molecular determinant that lies downstream of TH, and hierarchically mediates the TH-dependent EMT cascade. The E-box-binding transcription factor ZEB-1 is the master regulator of the EMT that acts by enhancing the migratory and invasive capacity of cancer cells by down-regulating epithelial markers [144], thereby promoting invasion and metastasis [145]. The transcriptional level, E-cadherin is the best-known negative target of ZEB-1 [148].

Moreover, ZEB-1 activates mesenchymal and stemness markers [144] thereby promoting tumorigenesis and metastasis in various human cancers [149-151]. As a repressor of E-cadherin, ZEB-1 is highly expressed in invasive carcinomas, at the invasive front of tumors in dedifferentiated cancer cells [151]. Here, we report that ZEB-1 is a downstream target of TH. This is in line with the finding that TH activation is a critical step towards invasiveness and metastatic conversion of SCC.

Accordingly, D3KO tumors have a high ZEB-1/E-cadherin ratio and are highly invasive (Figure 22 I).

In conclusion, in this study we addressed the central question of how TH influences different phases of tumorigenesis. Our data for the first time link in vitro mechanistic studies with a model of in vivo carcinogenesis in mice. By altering the TH signal via cell-specific deiodinase knock-down, we demonstrate that modulation of TH concentration can delay tumor cell growth and invasion depending on tumor stage and can affect the malignant epithelial tumor phenotype.

These findings not only transform our understanding of how T3 influences tumor progression, but also provides the rationale for the concept that pharmacologically induced TH inactivation could be a strategy with which to attenuate metastatic formations.

6. Materials and Methods

6.1 Cell cultures and transfections.

SCC-13 cells (Cellosaurus:RRID:CVCL_4029) were derived from skin squamous cell carcinoma (NCIt: C4819), SCC 011 (Cellosaurus: RRID:CVCL_5986) were derived from laryngeal squamous cell carcinoma (NCIt: C4044) and SCC 022 (Cellosaurus: RRID:CVCL_5991) were derived from laryngeal squamous cell carcinoma (NCIt: C4044). All the cells were myco- plasma free. SCC-13 and SCC D2KO cells were cultured in keratinocyte-SFM (KSFM 1×) serum-free medium [+] L-Glu (Gibco Life Technologies) with bovine pituitary extract (30 μg/ml) and human recombinant epidermal growth factor (EGF) protein (0.24 ng/ml). SCC D3KO cells were cultured in KSFM with 4% Ca^{2+}-chelated charcoal-stripped fetal bovine serum (FBS) and EGF human recombinant (Gibco Life Technologies). All transient transfections were performed using Lipofectamine 2000 (Life Technologies) according to the manufacturer's instructions.

6.2 Dio2 and Dio3 targeted mutagenesis.

Targeted mutagenesis of Dio3 and Dio2 in SCC was achieved by using the CRISPR/Cas9 system from Santa Cruz Bio- technology. Control SCC cells were stably transfected with the CRISPR/Cas9 control plasmid10. Three days after transfection with CRISPR/Cas9 plasmids, the cells were sorted using fluorescence-activated cell sorting (FACS) for green fluorescent protein expression. Single clones were analyzed by PCR to identify alterations in coding regions, and Dio2 exon 1 was sequenced to identify the inserted mutations. All the experiments in D2- and D3KO cells were repeated in three different D3KO and three different D2KO clones to avoid off-target effects.

6.3 Short hairpin RNA-mediated knockdown of ZEB-1.

SCC 13 cells were grown in p60 plates until they reached 60% confluence and then transfected with shRNA (targeting endogenous ZEB-1 or a non-targeting negative control using lipofectamine (Invitrogen). All the shRNA constructs were obtained from Thermo Fisher Scientific. Forty-eight hours after transfection, total protein lysate was collected and analyzed by Western blotting or total RNA was extracted and analyzed by real-time PCR. In parallel experiments, 24 h post-transfection, shRNA-transfected cells were used for scratch wound assays.

6.4 Real-time PCR.

Cells and tissues were lysed in Trizol (Life Technologies Ltd.) according to the manufacturer's protocol. 1 μg of total RNA was used to reverse transcribe cDNA using Vilo reverse transcriptase (Life Technologies Ltd.), followed by real-time qPCR using iQ5 Multicolor Real Time Detector System (BioRad) with the fluorescent double-stranded DNA-binding dye SYBR Green (Biorad).

Specific primers for each gene were designed to generate products of comparable sizes (about 200 bp for each amplification). For each reaction, standard curves for reference genes were constructed based on six four-fold serial dilutions of cDNA. All experiments were run in triplicate.

The gene expression levels were normalized to cyclophilin A and calculated as follows: N *target = 2(DCt sample–DCt calibrator). Primer sequences are indicated in the Table 3.

6.5 Protein extraction from skin and western blot analysis.

Dorsal skin was removed from mice and immediately snap-frozen in liquid N2. 800 μl of lysis buffer (0.125 M Tris pH 8.6; 3% SDS, protease inhibitors including PMSF 1 mM and phosphatase inhibitors) were added to all dorsal skin samples, which were then homogenized with Tissue Lyser (Qiagen). Total tissues protein or cell protein was separated by 10% SDS–PAGE followed by Western Blot. The membrane was then blocked with 5% non-fat dry milk in PBS, probed with anti-E-cadherin, anti-N-cadherin, anti-αFlag M2, anti-vimentin, anti-D3, and anti-tubulin antibodies (loading as control) overnight at 4 °C, washed, and incubated with horseradish peroxidase-conjugated anti-mouse immunoglobulin G secondary antibody (1:3000). Band detection was performed using an ECL kit (Millipore, cat. WBKLS0500). The gel images were analyzed using ImageJ software and all Western blot were run in triplicate. Antibodies are indicated in the Table 1.

6.6 Wound scratch assay.

SCC CTR, D2KO, and D3KO cells were seeded in p60 plates until they reached 100% confluence. Cells were then treated with mitomycin C from Streptomyces caespitotus (0.5 mg/ml). At time T0, a cross-shaped scratch was made on the cell monolayer with the tip of a sterile 2 μl micropipette. The FBS- free culture medium was then replaced with fresh medium to wash out released cells. Cell migration was measured by comparing pictures taken at the beginning and the end of the experiment at the times indicated in each experiment using ×10 magnification with a IX51 Olympus microscope and the Cell*F Olympus Imaging Software. ImageJ software

was used to draw the cell-free region limits in each case. The initial cell-free surface was subtracted from the endpoint cell-free surface and plotted in a graph as shown in Figures 17, 21.

6.7 Colony formation assay.

To evaluate colony formation, cells were seeded out in appropriate dilutions to form colonies. Five days after plating, cells were washed with PBS and stained with 1% crystal violet in 20% ethanol for 10 min at room temperature. Cells were washed twice with PBS and colonies were counted.

6.8 Invasion assay.

Matrigel chambers (Corning) were used to determine the effect of D3 depletion on invasiveness as per the manufacturer's protocol. In brief, SCC CTR, D2KO, and D3KO cells treated with T3 (30 nM) were harvested, re- suspended in serum-free medium, and then transferred to the hydrated Matrigel chambers (200,000 cells per well). The chambers were then incubated for 5 days in culture medium. The cells on the upper surface were scraped off and washed away, whereas the invaded cells on the lower surface were fixed and stained with 1% crystal violet in 20% ethanol for 10 min at room temperature. Finally, invaded cells and migrated cells were counted under a microscope and the relative number was calculated.

6.9 Matrix metalloproteinase (MMP) assays.

The concentrations of MMP-2, MMP- 3, MMP-7, and MMP-13 in the supernatant of SCC-CTR, SCC-CRISPD2, and SCC-CRISPD3 cells were detected via enzyme-linked assays (ELISA) according to the manufacturer's instructions (Cat. nos. ab100603; ab100606; ab100607; ab100608; ab100605). The absorbance at 450 nm was recorded using the VICTOR Multilabel Plate Reader. The general activity of the MMP enzyme was determined using an assay kit purchased from Abcam (Cat. no. ab112146) according to the manufacturer's protocol. In brief, SCC-CTR, SCC-CRISPD2, and SCC-CRISPD3 were seeded into triplicate wells of six-well plates and allowed to attach overnight and then starved with serum-free media for another 18 h. MMP activity was assayed in the media; 25 µl of medium was removed and added to 25 µl of 2 mM APMA working solution and incubated for 15 min at 20 °C after which 50 µl of the green substrate solution was added. An end-point measurement was then per- formed for the MMP activity using a microplate reader with a filter set of Ex/Em = 490/ 525 nm.

6.10 Chromatin immunoprecipitation (ChIP) assay.

ChIP Assays were performed in SCC13 cells after treatment with T3 and T4 (30 nM) for 48 h. Briefly, the cells were fixed with 1% formaldehyde for 10 min at 37 °C. The reaction was quenched by the addition of glycine to a final concentration of 0.125 M. After, cells were resus- pended in 1 ml of lysis buffer containing protease inhibitors (200 mM phenylmethylsulfony fluoride (PMSF), 1 μg/ml aprotinin) and sonicated to generate chromatin fragments of 200–1000 bp. An aliquot (1/10) of sheared chromatin was treated as Input DNA. Then, the sonicated chromatin was pre-cleared for 2 h with 1 μg of non-immune IgG (Calbiochem) and 30 μl of Protein G Plus/ Protein A Agarose suspension (Calbiochem) saturated with salmon sperm (1 mg/ml). After precleared chromatin was incubated at 4 °C for 16 h with 1 μg of anti-TRα. Protein/ DNA cross-links were reversed by incubation in 200 mM NaCl at 65 °C. Finally, DNA extraction was performed with phenol–chloroform and precipitated with ethanol. DNA fragments were used for real-time PCRs.

6.11 Tissue thyroid hormone levels.

Tumors T3 concentration was determined in frozen tissue with an LC–MS/MS method. The iodothyronines were measured with reversed phase chromatography (Waters BEH C18 column: 130 Å, 1.7 μm,
2.1 mm × 50 mm) on an Acquity UPLC-Xevo TQ-S tandem mass spectrometer system (Waters, Milford, MA, USA). Mobile phase A was acetonitrile:H2O:acetic acid 5:95:0.1, mobile phase B was acetonitrile:H2O:acetic acid 95:5:0.1. A gradient was applied with initial percentage B of 10%, which was increased linearly after 2.7 min to 40% in 5.6 min. Total runtime was 12 min. TH and internal standards were quantified using specific MRM transitions. All aspects of system operation and data acquisition were controlled using MassLynx, version 4.1 software with automated data processing using the TargetLynx Application Manager (Waters).

6.12 Animals, histology, and immunostaining.

sD3KO (K14CreERT-D3$^{fl/fl}$) mice were obtained by crossing the keratinocyte-specific conditional K14CreERT mouse [143] with D3fl/fl. Depletion was induced by treatment with 10 mg of tamoxifen at different time points as indicated in each experiment. The generation of D2-3xFlag is described else- where15. Skin lesions were harvested at different time points after tamoxifen administration and DMBA-TPA treatment. For immunofluorescence and histology, dorsal skin from sD3KO, D2-3xFlag, and control mice was embedded in paraffin, cut into 7-μm sections, and

H&E-stained. Slides were baked at 37 °C, deparaffinized by xylenes, dehydrated with ethanol, rehydrated in PBS, and permeabilized by placing them in 0.2% Triton X-100 in PBS. Antigens were retrieved by incubation in 0.1 M citrate buffer (pH 6.0) or 0.5 M Tris buffer (pH 8.0) at 95 °C for 5 min. Sections were blocked in 1% BSA/0.02% Tween/PBS for 1 h at room temperature. Primary antibodies were incubated overnight at 4 °C in blocking buffer and washed in 0.2% Tween/PBS. Secondary antibodies were incubated at room temperature for 1 h and washed in 0.2% Tween/PBS. Images were acquired with an IX51 Olympus microscope and the Cell*F Olympus Imaging Software.

6.13 DMBA/TPA carcinogenesis.

The dorsal skin of 2 months old mice was treated with a single dose (100 µl, 1 mg/ml) of the carcinogen 7,12-dimethylbenz[a]anthracene (DMBA) resuspended in propanone, followed by multiple applications of the tumor promoter 12-O-tetradecanoylphorbol-13-acetate, TPA (150 µl, 100 µM) in the two-stage protocol. Experiments in D3Fl/Fl mice were performed using 12 CTR mice and 12 sD3KO mice. Experiments in D2-Flag mice were performed using eight mice. In all the cohorts there were approximately as many females as male mice.

6.14 Animal study approval.

All animal studies were conducted in accordance with the guidelines of the Ministero della Salute and were approved by the Institutional Animal Care and Use Committee (IACUC, nos. 167/2015-PR and 354/2019-PR).

6.15 Statistics.

The data are expressed as means ± standard deviation (SD) of three independent experiments. Statistical differences and significance between samples were determined using the Student's two-tailed t test. Relative mRNA levels (in which the control sample was arbitrarily set as 1) are reported as results of real- time PCR, in which the expression of cyclophilin A served as housekeeping gene. A P value < 0.05 was considered statistically significant. Asterisks indicate significance at $*P < 0.05$, $**P < 0.01$, and $***P < 0.001$ throughout.

6.16 TABLE 1

List of Antibodies

ANTIBODIES	SOURCE	IDENTIFIER	DILUITION
Mouse monoclonal anti- E-cadherin	BD Biosciences	610181	1:500 IF 1:1000 WB
Rabbit polyclonal anti- N-cadherin	Elabscience	E-AB-32170	1:500 WB
Rabbit monoclonal anti-Vimentin	ABCAM	ab-92547	1:2000 WB 1:1000 IF
Rabbit polyclonal anti-αTubulin	Santa Cruz Biotecnology	SC-5546	1:10000 WB
Mouse monoclonal anti-αTubulin	Santa Cruz Biotecnology	SC-8035	1:10000 WB
Mouse monoclonal anti-FlagM2	SIGMA	Cat#F3165	1:1000 IF 1:1000 WB
Rabbit polyclonal anti-cytokeratin 14	COVANCE	D14IF01918	1:2000 IF
Rabbit polyclonal anti-CXCR4	ABCAM	ab-2074	1:300 IF
Rat anti-cytokeratin 8 (TROMA 1)	Hybridoma bank	AB_531826	1:300 IF
Anti-D3 718	Homemade	Homemade	1:500 IF 1:500 IHC
Anti-D3 717	Homemade	Homemade	1:500 WB
Anti-Phalloidin-TRITC labeled	SIGMA	77418-1EA	1:2000 IF
Rabbit polyclonal Anti-ZEB1	ABCAM	ab-155249	1:500 WB
Rabbit polyclonal Anti-ZEB1	Novus Bio	NBP1-05987	1:250 IF 1:250 IHC
Anti-Thyroid hormone receptor antibody (C3)-Chip Grade	ABCAM	ab-2743	2,5 μg
Anti-Thyroid hormone receptor beta antibody Chip Grade	ABCAM	ab-5622	2,5 μg
Rabbit polyclonal anti-GAPDH	Elabscience	E-AB-20059	1:5000 WB

6.17 TABLE 2

Gene list of the differentially regulated genes in the EMT RT² Profiler™ PCR Array

Refseq	Gene	Fold Change	Log2 Fold Change	p-Value
NM_000526	KRT14	0,3345	-1,579921884	0,000023
NM_004415	DSP	0,3856	-1,374823043	0,000137
NM_002276	KRT19	0,4005	-1,320125852	0,000001
NM_003239	TGFB3	0,446	-1,164884385	0,111945
NM_024060	AHNAK	0,4863	-1,040081503	0,0005
NM_006129	BMP1	0,4948	-1,015082595	0,000001
NM_033305	VPS13A	0,5471	-0,870123539	0,000083
NM_004360	CDH1	0,5586	-0,840112521	0,001817
NM_004949	DSC2	0,5844	-0,774971917	0,000033
NM_001982	ERBB3	0,5967	-0,744922318	0,000077
NM_003200	TCF3	0,6092	-0,715012153	0,000515
NM_004994	MMP9	0,6643	-0,59009318	0,01733
NM_002210	ITGAV	0,6736	-0,570035956	0,000013
NM_005607	PTK2	0,6807	-0,554908985	0,000002
NM_000660	TGFB1	0,6854	-0,544981903	0,002131
NM_002093	GSK3B	0,7071	-0,500013836	0,000004
NM_003199	TCF4	0,7071	-0,500013836	0,036101
NM_014399	TSPAN13	0,7711	-0,375010127	0,002593
NM_000474	TWIST1	0,7873	-0,345014617	0,00181
NM_002026	FN1	0,7928	-0,334971132	0,000014
NM_016946	F11R	0,8207	-0,285073142	0,014824
NM_000393	COL5A2	0,8409	-0,24999385	0,029895
NM_000125	ESR1	0,8526	-0,23005904	0,896521
NM_005163	AKT1	0,8615	-0,215077298	0,002433
NM_178031	TMEM132A	0,8675	-0,205064337	0,305309
NM_004626	WNT11	0,8675	-0,205064337	0,747444
NM_002923	RGS2	0,8736	-0,194955239	0,07424
NM_005901	SMAD2	0,895	-0,160040413	0,020305
NM_006908	RAC1	0,9044	-0,144967103	0,00155
NM_032642	WNT5B	0,9493	-0,075064012	0,829701
NM_002447	MST1R	0,9526	-0,070057546	0,57119
NM_003118	SPARC	0,9593	-0,059946038	0,060209
NM_001002	RPLP0	0,9626	-0,054991672	0,769718
NM_004530	MMP2	0,9693	-0,044984844	0,741577
NM_004342	CALD1	1	0	1
NM_004048	B2M	1	0	0,0014
NM_003254	TIMP1	1,007	0,010063683	0,929678
NM_015901	NUDT13	1,0105	0,015069322	0,696777
NM_002211	ITGB1	1,014	0,020057652	0,013697
NM_005228	EGFR	1,0281	0,039980598	0,249117
NM_001719	BMP7	1,0497	0,06997707	0,61614
NM_000577	IL1RN	1,057	0,079975377	0,607957
NM_001233	CAV2	1,0943	0,130008304	0,00036
NM_018584	CAMK2N1	1,1134	0,154971988	0,247466
NM_002046	GAPDH	1,1329	0,180020521	0,014804
NM_003463	PTP4A1	1,1408	0,190045887	0,005042
NM_178310	SNAI3	1,1487	0,200002066	0,416956
NM_003150	STAT3	1,2016	0,264956718	0,000008
NM_002609	PDGFRB	1,2184	0,284987847	0,144001
NM_003616	GEMIN2	1,2226	0,289952472	0,01184

NM_002422	MMP3	1,2527	0,325040955	0,135739
NM_018055	NODAL	1,2614	0,335025838	0,286391
NM_004517	ILK	1,2658	0,340049473	0,026201
NM_002444	MSN	1,2879	0,365020579	0,004024
NM_002538	OCLN	1,2968	0,374955996	0,001184
NM_000194	HPRT1	1,3059	0,385044426	0,000015
NM_006941	SOX10	1,3195	0,399991351	0,102928
NM_017617	NOTCH1	1,3472	0,429964044	0,244219
NM_001904	CTNNB1	1,366	0,449957484	0,011436
NM_173849	GSC	1,3803	0,464981862	0,208361
NM_015704	DESI1	1,4794	0,565012181	0,000065
NM_005251	FOXC2	1,521	0,605020153	0,120753
NM_005556	KRT7	1,5316	0,615039565	0,156949
NM_002205	ITGA5	1,5692	0,650029241	0,00003
NM_003507	FZD7	1,5746	0,654985383	0,004339
NM_003692	TMEFF1	1,5966	0,675002916	0,005836
NM_001101	ACTB	1,6021	0,679964201	0,000222
NM_005985	SNAI1	1,6133	0,690014739	0,113525
NM_003068	SNAI2	1,6301	0,704960471	0,000481
NM_001552	IGFBP4	1,676	0,745022149	0,17336
NM_003392	WNT5A	1,6818	0,75000615	0,135717
NM_000090	COL3A1	1,7411	0,799999066	0,102795
NM_012449	STEAP1	1,7532	0,809990584	0,020452
NM_000602	SERPINE1	1,8025	0,849999259	0,000001
NM_000214	JAG1	1,9656	0,974969763	0,005
NM_004126	GNG11	2,0209	1,014997935	0,000001
NM_016445	PLEK2	2,0209	1,014997935	0,000007
NM_000089	COL1A2	2,2191	1,149974682	0,017992
NM_003380	VIM	2,4368	1,284987847	0,003281
NM_014795	ZEB2	2,7606	1,464981862	0,022277
NM_003238	TGFB2	2,8879	1,530020787	0,000249
NM_000582	SPP1	3,5431	1,825012184	0,022297
NM_004385	VCAN	4,1267	2,044988562	0,006012
NM_006528	TFPI2	4,4537	2,155004382	0,000031
NM_001792	CDH2	5,0455	2,334997245	0,000063
NM_005130	FGFBP1	5,5212	2,464994927	0,090738
NM_001200	BMP2	6,0002	2,58501059	0,000171
NM_030751	ZEB1	7,3871	2,885008108	0,00023
NM_005909	MAP1B	8,0556	3,009992048	0,000033

6.18 TABLE 3

List of Oligonucleotides

Oligonucleotides used for real-time PCR		
Gene	**Forward primer (5' → 3')**	**Reverse primer (5' → 3')**
Cyclophilin A (CypA)	CGCCACTGTCGCTTTTCG	AACTTTGTCTGCAAACAGCTC
CYCLOPHILIN A (CYPA)	AGTCCATCTATGGGGAGAAATTTG	GCCTCCACAATATTCATGCCTTC
Dio2	CTTCCTCCTAGATGCCTACAAAC	GGCATAATTGTTACCTGATTCAGG
DIO2	CTCTATGACTCGGTCATTCTGC	TGTCACCTCCTTCTGTACTGG
Dio3	CCGCTCTCTGCTGCTTCAC	CGGATGCACAAGAAATCTAAAAGC
DIO3	CCTGGGACTCTGCTTCTGTAAC	GGGGTGTAAGAAAATGCTGTAGAG
E-cadherin (Cdh1)	CGTCCTGCCAATCCTGATGA	ACCACTGCCCTCGTAATCGAAC
E-CADHERIN (CDH1)	TGTCGACCGGTGCAATCTT	GGCGCCACCTCGAGAGA
Krt14	GATGTGACCTCCACCAACCG	CCATCGTGCACATCCATGAC
Krt6	TCGTGACCCTGAAGAAGGATGTA	CCTTGGCTTGCAGTTCAACTT
Krt8	ACAACAAGTTCGCCTCCTTC	TCTCCATCTCTGTACGCTTGT
MMP2	AAGGATGGCAAGTACGGCTT	TCATCGTAGTTGGCTGTGGT
MMP3	CTCCAACCGTGAGGAAAATC	CATGGAATTTCTCTTCTCATCAAA
MMP7	GGGGACTCCTACCCATTTGA	TTAGGATCAGAGGAATGTCC
MMP9	CCTGGAGACCTGAGAACCAATC	CGGCAAGTCTTCCGAGTAGT
MMP13	TCTTGTTGCTGCGCATGAGT	AAGGGTCACATTTGTCTGGC
N-cadherin (Cdh2)	ACAGTGGAGCTCTACAAAGG	CTGAGATGGGGTTGATAATG
N-CADHERIN (CDH2)	ACAGTGGCCACCTACAAAGG	CCGAGATGGGGTTGATAATG
TWIST	CCAGCTCCAGAGTCTCTAGA	GCCAGGTACATCGACTTCCT
VIM	GAACCTGCAGGAGGCAGAAG	CATCTTAACATTGAGCAGGTC
Oligonucleotides used for ChIP analysis		
Gene	**Forward primer (5' → 3')**	**Reverse primer (5' → 3')**
VIM	TGGTTCAGTCCCAGGCGGAC	CATGGTCCCGTTACTTCAGC
ZEB1	CGAGCATTTAGACACAAGCGA	CACTCACCGTTATTGCGCC
Oligonucleotides used for genome analysis		
Gene	**Forward primer (5' → 3')**	**Reverse primer (5' → 3')**
DIO3	GAGTCTCCCGCCAATTGAAG	AGCCCACCAAGTTCAGTCAA
Dio3	GTCTGGCTAACTTGAGACTCTGCT	TTGTCTTAGAACTAATCCCTTC
Dio2	TCAGAAGGAGACATTCTATTTC	AGGACAGAATCACTTCTTTCGCAA

7. References

1. Samarasinghe, V. and V. Madan, *Nonmelanoma skin cancer.* J Cutan Aesthet Surg, 2012. **5**(1): p. 3-10.
2. Ting, P.T., R. Kasper, and J.P. Arlette, *Metastatic basal cell carcinoma: report of two cases and literature review.* J Cutan Med Surg, 2005. **9**(1): p. 10-5.
3. van der Schroeff, J.G., et al., *Ras oncogene mutations in basal cell carcinomas and squamous cell carcinomas of human skin.* J Invest Dermatol, 1990. **94**(4): p. 423-5.
4. Ratushny, V., et al., *From keratinocyte to cancer: the pathogenesis and modeling of cutaneous squamous cell carcinoma.* J Clin Invest, 2012. **122**(2): p. 464-72.
5. Karia, P.S., J. Han, and C.D. Schmults, *Cutaneous squamous cell carcinoma: estimated incidence of disease, nodal metastasis, and deaths from disease in the United States, 2012.* J Am Acad Dermatol, 2013. **68**(6): p. 957-66.
6. Alam, M. and D. Ratner, *Cutaneous squamous-cell carcinoma.* N Engl J Med, 2001. **344**(13): p. 975-83.
7. Cockerell, C.J., *Histopathology of incipient intraepidermal squamous cell carcinoma ("actinic keratosis").* J Am Acad Dermatol, 2000. **42**(1 Pt 2): p. 11-7.
8. Marks, R., G. Rennie, and T.S. Selwood, *Malignant transformation of solar keratoses to squamous cell carcinoma.* Lancet, 1988. **1**(8589): p. 795-7.
9. Criscione, V.D., et al., *Actinic keratoses: Natural history and risk of malignant transformation in the Veterans Affairs Topical Tretinoin Chemoprevention Trial.* Cancer, 2009. **115**(11): p. 2523-30.
10. Ziegler, A., et al., *Sunburn and p53 in the onset of skin cancer.* Nature, 1994. **372**(6508): p. 773-6.
11. Ortonne, J.P., *From actinic keratosis to squamous cell carcinoma.* Br J Dermatol, 2002. **146 Suppl 61**: p. 20-3.
12. Nakazawa, H., et al., *UV and skin cancer: specific p53 gene mutation in normal skin as a biologically relevant exposure measurement.* Proc Natl Acad Sci U S A, 1994. **91**(1): p. 360-4.
13. Hoeijmakers, J.H., *Genome maintenance mechanisms for preventing cancer.* Nature, 2001. **411**(6835): p. 366-74.
14. Brash, D.E., et al., *A role for sunlight in skin cancer: UV-induced p53 mutations in squamous cell carcinoma.* Proc Natl Acad Sci U S A, 1991. **88**(22): p. 10124-8.
15. Donehower, L.A., et al., *Mice deficient for p53 are developmentally normal but susceptible to spontaneous tumours.* Nature, 1992. **356**(6366): p. 215-21.
16. Jiang, W., et al., *p53 protects against skin cancer induction by UV-B radiation.* Oncogene, 1999. **18**(29): p. 4247-53.
17. Owens, D.M. and F.M. Watt, *Contribution of stem cells and differentiated cells to epidermal tumours.* Nat Rev Cancer, 2003. **3**(6): p. 444-51.
18. Kemp, C.J., *Multistep skin cancer in mice as a model to study the evolution of cancer cells.* Semin Cancer Biol, 2005. **15**(6): p. 460-73.
19. Quintanilla, M., et al., *Carcinogen-specific mutation and amplification of Ha-ras during mouse skin carcinogenesis.* Nature, 1986. **322**(6074): p. 78-80.

20. Spencer, J.M., et al., *Activated ras genes occur in human actinic keratoses, premalignant precursors to squamous cell carcinomas.* Arch Dermatol, 1995. **131**(7): p. 796-800.
21. Sutter, C., et al., *ras gene activation and aberrant expression of keratin K13 in ultraviolet B radiation-induced epidermal neoplasias of mouse skin.* Mol Carcinog, 1993. **8**(1): p. 13-9.
22. Perez-Losada, J. and A. Balmain, *Stem-cell hierarchy in skin cancer.* Nat Rev Cancer, 2003. **3**(6): p. 434-43.
23. Boutwell, R.K., et al., *Mouse skin: a useful model system for studying the mechanism of chemical carcinogenesis.* Carcinog Compr Surv, 1982. **7**: p. 1-12.
24. Hay, E.D., *An overview of epithelio-mesenchymal transformation.* Acta Anat (Basel), 1995. **154**(1): p. 8-20.
25. Thiery, J.P. and J.P. Sleeman, *Complex networks orchestrate epithelial-mesenchymal transitions.* Nat Rev Mol Cell Biol, 2006. **7**(2): p. 131-42.
26. Thiery, J.P., et al., *Epithelial-mesenchymal transitions in development and disease.* Cell, 2009. **139**(5): p. 871-90.
27. Huang, R.Y., P. Guilford, and J.P. Thiery, *Early events in cell adhesion and polarity during epithelial-mesenchymal transition.* J Cell Sci, 2012. **125**(Pt 19): p. 4417-22.
28. Peinado, H., D. Olmeda, and A. Cano, *Snail, Zeb and bHLH factors in tumour progression: an alliance against the epithelial phenotype?* Nat Rev Cancer, 2007. **7**(6): p. 415-28.
29. Yilmaz, M. and G. Christofori, *EMT, the cytoskeleton, and cancer cell invasion.* Cancer Metastasis Rev, 2009. **28**(1-2): p. 15-33.
30. Hansen, S.M., V. Berezin, and E. Bock, *Signaling mechanisms of neurite outgrowth induced by the cell adhesion molecules NCAM and N-cadherin.* Cell Mol Life Sci, 2008. **65**(23): p. 3809-21.
31. Nistico, P., M.J. Bissell, and D.C. Radisky, *Epithelial-mesenchymal transition: general principles and pathological relevance with special emphasis on the role of matrix metalloproteinases.* Cold Spring Harb Perspect Biol, 2012. **4**(2).
32. Sheppard, D., *Integrin-mediated activation of latent transforming growth factor beta.* Cancer Metastasis Rev, 2005. **24**(3): p. 395-402.
33. De Craene, B. and G. Berx, *Regulatory networks defining EMT during cancer initiation and progression.* Nat Rev Cancer, 2013. **13**(2): p. 97-110.
34. Zhang, P., Y. Sun, and L. Ma, *ZEB1: at the crossroads of epithelial-mesenchymal transition, metastasis and therapy resistance.* Cell Cycle, 2015. **14**(4): p. 481-7.
35. Kahlert, U.D., et al., *Activation of canonical WNT/beta-catenin signaling enhances in vitro motility of glioblastoma cells by activation of ZEB1 and other activators of epithelial-to-mesenchymal transition.* Cancer Lett, 2012. **325**(1): p. 42-53.
36. Chua, H.L., et al., *NF-kappaB represses E-cadherin expression and enhances epithelial to mesenchymal transition of mammary epithelial cells: potential involvement of ZEB-1 and ZEB-2.* Oncogene, 2007. **26**(5): p. 711-24.
37. Horiguchi, K., et al., *TGF-beta drives epithelial-mesenchymal transition through deltaEF1-mediated downregulation of ESRP.* Oncogene, 2012. **31**(26): p. 3190-201.

38. Dohadwala, M., et al., *Cyclooxygenase-2-dependent regulation of E-cadherin: prostaglandin E(2) induces transcriptional repressors ZEB1 and snail in non-small cell lung cancer.* Cancer Res, 2006. **66**(10): p. 5338-45.
39. Krishnamachary, B., et al., *Hypoxia-inducible factor-1-dependent repression of E-cadherin in von Hippel-Lindau tumor suppressor-null renal cell carcinoma mediated by TCF3, ZFHX1A, and ZFHX1B.* Cancer Res, 2006. **66**(5): p. 2725-31.
40. Korpal, M., et al., *The miR-200 family inhibits epithelial-mesenchymal transition and cancer cell migration by direct targeting of E-cadherin transcriptional repressors ZEB1 and ZEB2.* J Biol Chem, 2008. **283**(22): p. 14910-4.
41. Park, S.M., et al., *The miR-200 family determines the epithelial phenotype of cancer cells by targeting the E-cadherin repressors ZEB1 and ZEB2.* Genes Dev, 2008. **22**(7): p. 894-907.
42. Postigo, A.A., *Opposing functions of ZEB proteins in the regulation of the TGFbeta/BMP signaling pathway.* EMBO J, 2003. **22**(10): p. 2443-52.
43. Eger, A., et al., *DeltaEF1 is a transcriptional repressor of E-cadherin and regulates epithelial plasticity in breast cancer cells.* Oncogene, 2005. **24**(14): p. 2375-85.
44. Shi, Y., et al., *Coordinated histone modifications mediated by a CtBP co-repressor complex.* Nature, 2003. **422**(6933): p. 735-8.
45. Sanchez-Tillo, E., et al., *ZEB1 represses E-cadherin and induces an EMT by recruiting the SWI/SNF chromatin-remodeling protein BRG1.* Oncogene, 2010. **29**(24): p. 3490-500.
46. Postigo, A.A., et al., *Regulation of Smad signaling through a differential recruitment of coactivators and corepressors by ZEB proteins.* EMBO J, 2003. **22**(10): p. 2453-62.
47. Mendoza, A. and A.N. Hollenberg, *New insights into thyroid hormone action.* Pharmacol Ther, 2017. **173**: p. 135-145.
48. Gereben, B., et al., *Cellular and molecular basis of deiodinase-regulated thyroid hormone signaling.* Endocr Rev, 2008. **29**(7): p. 898-938.
49. Nillni, E.A., *Regulation of the hypothalamic thyrotropin releasing hormone (TRH) neuron by neuronal and peripheral inputs.* Front Neuroendocrinol, 2010. **31**(2): p. 134-56.
50. Cheng, S.Y., J.L. Leonard, and P.J. Davis, *Molecular aspects of thyroid hormone actions.* Endocr Rev, 2010. **31**(2): p. 139-70.
51. Visser, W.E., et al., *The thyroid hormone transporters MCT8 and MCT10 transport the affinity-label N-bromoacetyl-[(125)I]T3 but are not modified by it.* Mol Cell Endocrinol, 2011. **337**(1-2): p. 96-100.
52. Visser, W.E., et al., *Thyroid hormone transport in and out of cells.* Trends Endocrinol Metab, 2008. **19**(2): p. 50-6.
53. Abe, T., et al., *Molecular characterization and tissue distribution of a new organic anion transporter subtype (oatp3) that transports thyroid hormones and taurocholate and comparison with oatp2.* J Biol Chem, 1998. **273**(35): p. 22395-401.
54. Schweizer, U. and J. Kohrle, *Function of thyroid hormone transporters in the central nervous system.* Biochim Biophys Acta, 2013. **1830**(7): p. 3965-73.

55. Dumitrescu, A.M., et al., *A novel syndrome combining thyroid and neurological abnormalities is associated with mutations in a monocarboxylate transporter gene.* Am J Hum Genet, 2004. **74**(1): p. 168-75.
56. Alkemade, A., et al., *Thyroid hormone receptor expression in the human hypothalamus and anterior pituitary.* J Clin Endocrinol Metab, 2005. **90**(2): p. 904-12.
57. Heuer, H., et al., *The monocarboxylate transporter 8 linked to human psychomotor retardation is highly expressed in thyroid hormone-sensitive neuron populations.* Endocrinology, 2005. **146**(4): p. 1701-6.
58. Kohrle, J., *The deiodinase family: selenoenzymes regulating thyroid hormone availability and action.* Cell Mol Life Sci, 2000. **57**(13-14): p. 1853-63.
59. Arrojo, E.D.R. and A.C. Bianco, *Type 2 deiodinase at the crossroads of thyroid hormone action.* Int J Biochem Cell Biol, 2011. **43**(10): p. 1432-41.
60. Curcio-Morelli, C., et al., *Deubiquitination of type 2 iodothyronine deiodinase by von Hippel-Lindau protein-interacting deubiquitinating enzymes regulates thyroid hormone activation.* J Clin Invest, 2003. **112**(2): p. 189-96.
61. Sagar, G.D., et al., *The thyroid hormone-inactivating deiodinase functions as a homodimer.* Mol Endocrinol, 2008. **22**(6): p. 1382-93.
62. Schneider, M.J., et al., *Targeted disruption of the type 1 selenodeiodinase gene (Dio1) results in marked changes in thyroid hormone economy in mice.* Endocrinology, 2006. **147**(1): p. 580-9.
63. Burmeister, L.A., J. Pachucki, and D.L. St Germain, *Thyroid hormones inhibit type 2 iodothyronine deiodinase in the rat cerebral cortex by both pre- and posttranslational mechanisms.* Endocrinology, 1997. **138**(12): p. 5231-7.
64. Bianco, A.C., et al., *Biochemistry, cellular and molecular biology, and physiological roles of the iodothyronine selenodeiodinases.* Endocr Rev, 2002. **23**(1): p. 38-89.
65. Williams, G.R. and J.H. Bassett, *Deiodinases: the balance of thyroid hormone: local control of thyroid hormone action: role of type 2 deiodinase.* J Endocrinol, 2011. **209**(3): p. 261-72.
66. Gereben, B., et al., *Activation and inactivation of thyroid hormone by deiodinases: local action with general consequences.* Cell Mol Life Sci, 2008. **65**(4): p. 570-90.
67. Dentice, M., D. Antonini, and D. Salvatore, *Type 3 deiodinase and solid tumors: an intriguing pair.* Expert Opin Ther Targets, 2013. **17**(11): p. 1369-79.
68. Dentice, M. and D. Salvatore, *Deiodinases: the balance of thyroid hormone: local impact of thyroid hormone inactivation.* J Endocrinol, 2011. **209**(3): p. 273-82.
69. Lazar, M.A., *Thyroid hormone action: a binding contract.* J Clin Invest, 2003. **112**(4): p. 497-9.
70. Brent, G.A., *Mechanisms of thyroid hormone action.* J Clin Invest, 2012. **122**(9): p. 3035-43.
71. Flamant, F., et al., *Thyroid Hormone Signaling Pathways: Time for a More Precise Nomenclature.* Endocrinology, 2017. **158**(7): p. 2052-2057.
72. Proksch, E., J.M. Brandner, and J.M. Jensen, *The skin: an indispensable barrier.* Exp Dermatol, 2008. **17**(12): p. 1063-72.
73. Moll, R., M. Divo, and L. Langbein, *The human keratins: biology and pathology.* Histochem Cell Biol, 2008. **129**(6): p. 705-33.

74. Dai, X. and J.A. Segre, *Transcriptional control of epidermal specification and differentiation.* Curr Opin Genet Dev, 2004. **14**(5): p. 485-91.
75. Krueger, G.G. and G. Stingl, *Immunology/inflammation of the skin--a 50-year perspective.* J Invest Dermatol, 1989. **92**(4 Suppl): p. 32S-51S.
76. Antonini, D., et al., *An Intimate Relationship between Thyroid Hormone and Skin: Regulation of Gene Expression.* Front Endocrinol (Lausanne), 2013. **4**: p. 104.
77. Luongo, C., M. Dentice, and D. Salvatore, *Deiodinases and their intricate role in thyroid hormone homeostasis.* Nat Rev Endocrinol, 2019. **15**(8): p. 479-488.
78. Furlow, J.D. and E.S. Neff, *A developmental switch induced by thyroid hormone: Xenopus laevis metamorphosis.* Trends Endocrinol Metab, 2006. **17**(2): p. 40-7.
79. Safer, J.D., *Thyroid hormone and wound healing.* J Thyroid Res, 2013. **2013**: p. 124538.
80. Safer, J.D., T.M. Crawford, and M.F. Holick, *Topical thyroid hormone accelerates wound healing in mice.* Endocrinology, 2005. **146**(10): p. 4425-30.
81. Dentice, M., et al., *Sonic hedgehog-induced type 3 deiodinase blocks thyroid hormone action enhancing proliferation of normal and malignant keratinocytes.* Proc Natl Acad Sci U S A, 2007. **104**(36): p. 14466-71.
82. Ramot, Y., et al., *Endocrine controls of keratin expression.* Bioessays, 2009. **31**(4): p. 389-99.
83. Mathisen, P.M. and L. Miller, *Thyroid hormone induces constitutive keratin gene expression during Xenopus laevis development.* Mol Cell Biol, 1989. **9**(5): p. 1823-31.
84. van Beek, N., et al., *Thyroid hormones directly alter human hair follicle functions: anagen prolongation and stimulation of both hair matrix keratinocyte proliferation and hair pigmentation.* J Clin Endocrinol Metab, 2008. **93**(11): p. 4381-8.
85. Tomic-Canic, M., et al., *Novel regulation of keratin gene expression by thyroid hormone and retinoid receptors.* J Biol Chem, 1996. **271**(3): p. 1416-23.
86. Jho, S.H., et al., *The book of opposites: the role of the nuclear receptor co-regulators in the suppression of epidermal genes by retinoic acid and thyroid hormone receptors.* J Invest Dermatol, 2005. **124**(5): p. 1034-43.
87. Tomic-Canic, M., et al., *Identification of the retinoic acid and thyroid hormone receptor-responsive element in the human K14 keratin gene.* J Invest Dermatol, 1992. **99**(6): p. 842-7.
88. Jho, S.H., et al., *Negative response elements in keratin genes mediate transcriptional repression and the cross-talk among nuclear receptors.* J Biol Chem, 2001. **276**(49): p. 45914-20.
89. Radoja, N., et al., *Specific organization of the negative response elements for retinoic acid and thyroid hormone receptors in keratin gene family.* J Invest Dermatol, 1997. **109**(4): p. 566-72.
90. Radoja, N., et al., *Thyroid hormones and gamma interferon specifically increase K15 keratin gene transcription.* Mol Cell Biol, 2004. **24**(8): p. 3168-79.
91. Slominski, A. and J. Wortsman, *Neuroendocrinology of the skin.* Endocr Rev, 2000. **21**(5): p. 457-87.
92. Leonhardt, J.M. and W.R. Heymann, *Thyroid disease and the skin.* Dermatol Clin, 2002. **20**(3): p. 473-81, vii.

93. Hernandez, A. and D.L. St Germain, *Dexamethasone inhibits growth factor-induced type 3 deiodinase activity and mRNA expression in a cultured cell line derived from rat neonatal brown fat vascular-stromal cells.* Endocrinology, 2002. **143**(7): p. 2652-8.
94. Tujebajeva, R.M., et al., *Decoding apparatus for eukaryotic selenocysteine insertion.* EMBO Rep, 2000. **1**(2): p. 158-63.
95. Hernandez, A., et al., *The gene locus encoding iodothyronine deiodinase type 3 (Dio3) is imprinted in the fetus and expresses antisense transcripts.* Endocrinology, 2002. **143**(11): p. 4483-6.
96. Kaplan, M.M. and K.A. Yaskoski, *Phenolic and tyrosyl ring deiodination of iodothyronines in rat brain homogenates.* J Clin Invest, 1980. **66**(3): p. 551-62.
97. Bates, J.M., D.L. St Germain, and V.A. Galton, *Expression profiles of the three iodothyronine deiodinases, D1, D2, and D3, in the developing rat.* Endocrinology, 1999. **140**(2): p. 844-51.
98. Galton, V.A., et al., *Pregnant rat uterus expresses high levels of the type 3 iodothyronine deiodinase.* J Clin Invest, 1999. **103**(7): p. 979-87.
99. Brown, D.D., et al., *Thyroid hormone controls multiple independent programs required for limb development in Xenopus laevis metamorphosis.* Proc Natl Acad Sci U S A, 2005. **102**(35): p. 12455-8.
100. Huang, S.A., et al., *Type 3 iodothyronine deiodinase is highly expressed in the human uteroplacental unit and in fetal epithelium.* J Clin Endocrinol Metab, 2003. **88**(3): p. 1384-8.
101. Olivares, E.L., et al., *Thyroid function disturbance and type 3 iodothyronine deiodinase induction after myocardial infarction in rats a time course study.* Endocrinology, 2007. **148**(10): p. 4786-92.
102. Dentice, M., et al., *beta-Catenin regulates deiodinase levels and thyroid hormone signaling in colon cancer cells.* Gastroenterology, 2012. **143**(4): p. 1037-47.
103. Catalano, V., et al., *Activated Thyroid Hormone Promotes Differentiation and Chemotherapeutic Sensitization of Colorectal Cancer Stem Cells by Regulating Wnt and BMP4 Signaling.* Cancer Res, 2016. **76**(5): p. 1237-44.
104. Luongo, C., et al., *The sonic hedgehog-induced type 3 deiodinase facilitates tumorigenesis of basal cell carcinoma by reducing Gli2 inactivation.* Endocrinology, 2014. **155**(6): p. 2077-88.
105. Sirakov, M., et al., *The thyroid hormone nuclear receptor TRalpha1 controls the Notch signaling pathway and cell fate in murine intestine.* Development, 2015. **142**(16): p. 2764-74.
106. Hiroi, Y., et al., *Rapid nongenomic actions of thyroid hormone.* Proc Natl Acad Sci U S A, 2006. **103**(38): p. 14104-9.
107. Garcia-Silva, S. and A. Aranda, *The thyroid hormone receptor is a suppressor of ras-mediated transcription, proliferation, and transformation.* Mol Cell Biol, 2004. **24**(17): p. 7514-23.
108. Miro, C., et al., *The Concerted Action of Type 2 and Type 3 Deiodinases Regulates the Cell Cycle and Survival of Basal Cell Carcinoma Cells.* Thyroid, 2017. **27**(4): p. 567-576.
109. Gailani, M.R., et al., *The role of the human homologue of Drosophila patched in sporadic basal cell carcinomas.* Nat Genet, 1996. **14**(1): p. 78-81.

110. Kasper, M., et al., *Basal cell carcinoma - molecular biology and potential new therapies.* J Clin Invest, 2012. **122**(2): p. 455-63.
111. Oro, A.E., et al., *Basal cell carcinomas in mice overexpressing sonic hedgehog.* Science, 1997. **276**(5313): p. 817-21.
112. Xie, J., et al., *Activating Smoothened mutations in sporadic basal-cell carcinoma.* Nature, 1998. **391**(6662): p. 90-2.
113. Volinia, S., et al., *A microRNA expression signature of human solid tumors defines cancer gene targets.* Proc Natl Acad Sci U S A, 2006. **103**(7): p. 2257-61.
114. Chan, J.A., A.M. Krichevsky, and K.S. Kosik, *MicroRNA-21 is an antiapoptotic factor in human glioblastoma cells.* Cancer Res, 2005. **65**(14): p. 6029-33.
115. Xu, L.F., et al., *MicroRNA-21 (miR-21) regulates cellular proliferation, invasion, migration, and apoptosis by targeting PTEN, RECK and Bcl-2 in lung squamous carcinoma, Gejiu City, China.* PLoS One, 2014. **9**(8): p. e103698.
116. Lv, L., et al., *MicroRNA-21 is overexpressed in renal cell carcinoma.* Int J Biol Markers, 2013. **28**(2): p. 201-7.
117. Hiyoshi, Y., et al., *MicroRNA-21 regulates the proliferation and invasion in esophageal squamous cell carcinoma.* Clin Cancer Res, 2009. **15**(6): p. 1915-22.
118. Li, X., K. Huang, and J. Yu, *Inhibition of microRNA-21 upregulates the expression of programmed cell death 4 and phosphatase tensin homologue in the A431 squamous cell carcinoma cell line.* Oncol Lett, 2014. **8**(1): p. 203-207.
119. Asangani, I.A., et al., *MicroRNA-21 (miR-21) post-transcriptionally downregulates tumor suppressor Pdcd4 and stimulates invasion, intravasation and metastasis in colorectal cancer.* Oncogene, 2008. **27**(15): p. 2128-36.
120. Ren, W., et al., *MiR-21 modulates chemosensitivity of tongue squamous cell carcinoma cells to cisplatin by targeting PDCD4.* Mol Cell Biochem, 2014. **390**(1-2): p. 253-62.
121. Wong, S.Y. and A.A. Dlugosz, *Basal cell carcinoma, Hedgehog signaling, and targeted therapeutics: the long and winding road.* J Invest Dermatol, 2014. **134**(e1): p. E18-22.
122. Di Girolamo, D., et al., *Reciprocal interplay between thyroid hormone and microRNA-21 regulates hedgehog pathway-driven skin tumorigenesis.* J Clin Invest, 2016. **126**(6): p. 2308-20.
123. Cao, Z., et al., *PDCD4 expression inversely correlated with miR-21 levels in gastric cancers.* J Cancer Res Clin Oncol, 2012. **138**(4): p. 611-9.
124. Morrisey, E.E., *The magic and mystery of miR-21.* J Clin Invest, 2010. **120**(11): p. 3817-9.
125. Hildebrand, J., et al., *A comprehensive analysis of microRNA expression during human keratinocyte differentiation in vitro and in vivo.* J Invest Dermatol, 2011. **131**(1): p. 20-9.
126. Yi, R., et al., *Morphogenesis in skin is governed by discrete sets of differentially expressed microRNAs.* Nat Genet, 2006. **38**(3): p. 356-62.
127. Ahmed, M.I., et al., *MicroRNA-21 is an important downstream component of BMP signalling in epidermal keratinocytes.* J Cell Sci, 2011. **124**(Pt 20): p. 3399-404.
128. Joyce, C.E., et al., *Deep sequencing of small RNAs from human skin reveals major alterations in the psoriasis miRNAome.* Hum Mol Genet, 2011. **20**(20): p. 4025-40.

129. Zibert, J.R., et al., *MicroRNAs and potential target interactions in psoriasis.* J Dermatol Sci, 2010. **58**(3): p. 177-85.
130. Dziunycz, P., et al., *Squamous cell carcinoma of the skin shows a distinct microRNA profile modulated by UV radiation.* J Invest Dermatol, 2010. **130**(11): p. 2686-9.
131. Akagi, I., et al., *Relationship between altered expression levels of MIR21, MIR143, MIR145, and MIR205 and clinicopathologic features of esophageal squamous cell carcinoma.* Dis Esophagus, 2011. **24**(7): p. 523-30.
132. Satzger, I., et al., *microRNA-21 is upregulated in malignant melanoma and influences apoptosis of melanocytic cells.* Exp Dermatol, 2012. **21**(7): p. 509-14.
133. Stramer, B. and P. Martin, *Cell biology: master regulators of sealing and healing.* Curr Biol, 2005. **15**(11): p. R425-7.
134. Darido, C., et al., *Targeting of the tumor suppressor GRHL3 by a miR-21-dependent proto-oncogenic network results in PTEN loss and tumorigenesis.* Cancer Cell, 2011. **20**(5): p. 635-48.
135. Yu, Z., et al., *The Grainyhead-like epithelial transactivator Get-1/Grhl3 regulates epidermal terminal differentiation and interacts functionally with LMO4.* Dev Biol, 2006. **299**(1): p. 122-36.
136. Bhandari, A., et al., *The Grainyhead transcription factor Grhl3/Get1 suppresses miR-21 expression and tumorigenesis in skin: modulation of the miR-21 target MSH2 by RNA-binding protein DND1.* Oncogene, 2013. **32**(12): p. 1497-507.
137. Cicatiello, A.G., R. Ambrosio, and M. Dentice, *Thyroid hormone promotes differentiation of colon cancer stem cells.* Mol Cell Endocrinol, 2017. **459**: p. 84-89.
138. Huang, P.Y. and A. Balmain, *Modeling cutaneous squamous carcinoma development in the mouse.* Cold Spring Harb Perspect Med, 2014. **4**(9): p. a013623.
139. Castagna, M.G., et al., *DIO2 Thr92Ala Reduces Deiodinase-2 Activity and Serum-T3 Levels in Thyroid-Deficient Patients.* J Clin Endocrinol Metab, 2017. **102**(5): p. 1623-1630.
140. Yuspa, S.H. and M.C. Poirier, *Chemical carcinogenesis: from animal models to molecular models in one decade.* Adv Cancer Res, 1988. **50**: p. 25-70.
141. Tomakidi, P., et al., *Discriminating expression of differentiation markers evolves in transplants of benign and malignant human skin keratinocytes through stromal interactions.* J Pathol, 2003. **200**(3): p. 298-307.
142. Dentice, M., et al., *Intracellular inactivation of thyroid hormone is a survival mechanism for muscle stem cell proliferation and lineage progression.* Cell Metab, 2014. **20**(6): p. 1038-48.
143. Lapouge, G., et al., *Skin squamous cell carcinoma propagating cells increase with tumour progression and invasiveness.* EMBO J, 2012. **31**(24): p. 4563-75.
144. Brabletz, S. and T. Brabletz, *The ZEB/miR-200 feedback loop--a motor of cellular plasticity in development and cancer?* EMBO Rep, 2010. **11**(9): p. 670-7.
145. Caramel, J., M. Ligier, and A. Puisieux, *Pleiotropic Roles for ZEB1 in Cancer.* Cancer Res, 2018. **78**(1): p. 30-35.
146. Luongo, C., et al., *The selective loss of the type 2 iodothyronine deiodinase in mouse thyrotrophs increases basal TSH but blunts the thyrotropin response to hypothyroidism.* Endocrinology, 2015. **156**(2): p. 745-54.

147. Friedl, P. and K. Wolf, *Tumour-cell invasion and migration: diversity and escape mechanisms.* Nat Rev Cancer, 2003. **3**(5): p. 362-74.
148. Gemmill, R.M., et al., *ZEB1-responsive genes in non-small cell lung cancer.* Cancer Lett, 2011. **300**(1): p. 66-78.
149. Sanchez-Tillo, E., et al., *EMT-activating transcription factors in cancer: beyond EMT and tumor invasiveness.* Cell Mol Life Sci, 2012. **69**(20): p. 3429-56.
150. Wellner, U., et al., *The EMT-activator ZEB1 promotes tumorigenicity by repressing stemness-inhibiting microRNAs.* Nat Cell Biol, 2009. **11**(12): p. 1487-95.
151. Spaderna, S., et al., *The transcriptional repressor ZEB1 promotes metastasis and loss of cell polarity in cancer.* Cancer Res, 2008. **68**(2): p. 537-44.